Final draft of paper

M. Pontani, F. Celani. Lunar ascent and orbit injection via neighboring optimal guidance and constrained attitude control. Journal of Aerospace Engineering. 31(5):04018071-1 - 04018071-11, September 2018. doi:10.1061/(ASCE)AS.1943-5525.0000908

Lunar Ascent and Orbit Injection via Neighboring Optimal Guidance and Constrained Attitude Control

Mauro Pontani[1] and Fabio Celani[2]

[1] Assistant Professor, Department of Astronautical, Electrical, and Energy Engineering, Sapienza University of Rome, via Salaria 851, 00138 Rome, Italy. Email mauro.pontani@uniroma1.it.

[2] Assistant Professor, School of Aerospace Engineering, Sapienza University of Rome, via Salaria 851, 00138 Rome, Italy

ABSTRACT

Future human or robotic missions to the Moon will require efficient ascent path and accurate orbit injection maneuvers, because the dynamical conditions at injection affect the subsequent phases of spaceflight. This research is focused on the original combination of two techniques applied to lunar ascent modules, i.e. (i) the recently-introduced variable-time-domain neighboring optimal guidance (VTD-NOG), and (ii) a constrained proportional-derivative (CPD) attitude control algorithm. VTD-NOG belongs to the class of feedback implicit guidance approaches, aimed at finding the corrective control actions capable of maintaining the spacecraft sufficiently close to the reference trajectory. CPD pursues the desired attitude using thrust vector control, while constraining the rate of the thrust deflection angle. The numerical results unequivocally demonstrate that the joint use of VTD-NOG and CPD represents an accurate and effective methodology for guidance and control of lunar ascent path and orbit injection, in the presence of nonnominal flight conditions .

INTRODUCTION

In the last decades, manned and automatic lunar missions have attracted an increasing interest by many countries. Building a lunar base for future interplanetary missions represents only one of several challenging

projects. The development of a reliable guidance and control algorithm for automatic lunar descent, ascent, and orbit injection represents a crucial issue for a safe connection between Earth and Moon.

In the scientific literature, only a limited number of works dealt with the joint application of guidance and control (G&C) algorithms to aerospace vehicles. Geller 2006 employs proportional-derivative (PD) control for both guidance and control algorithms. Guidance and control based on Nonlinear Dynamic Inversion is studied by Marcos et al. 2008, and a comparison between Dynamic Inversion and State Dependent Riccati Equation approaches is presented in Lam et al. 2008. Integrated G&C methods are proposed in Tian et al. 2015a and in Tian et al. 2015b, while the use of G&C based on sliding-mode is investigated in Yeh 2015.

This research is focused on the original combination of two techniques applied to two-dimensional lunar ascent paths, i.e. (i) the recently-introduced (Pontani et al. 2015a, Pontani et al. 2015b, Pontani et al. 2015c, and Pontani 2016) variable-time-domain neighboring optimal guidance (VTD-NOG), and (ii) a constrained proportional-derivative (CPD) attitude control algorithm. VTD-NOG belongs to the class of feedback implicit guidance approaches (cf. Lu 1991, Kugelmann and Pesch 1990a, and Kugelmann and Pesch 1990b), aimed at finding the corrective control actions capable of maintaining the spacecraft sufficiently close to the reference path. This is an optimal trajectory that fulfills the second-order analytical conditions for optimality, similarly to what occurs for alternative neighboring optimal guidance (NOG) schemes. Only a limited number of researches have been focused on NOG (Afshari et al. 2009, Seywald and Cliff 1994, Yan et al. 2002, Charalambous et al. 1995, Hull 2003, and Hull and Novak 1993). Former NOG algorithms exhibit a common difficulty, which is represented by singularities of the gain matrices while approaching the final time. A fundamental original feature of VTD-NOG is the use of a normalized time scale for the definition of the nominal trajectory and the related vectors and matrices. As a result, the gain matrices do not diverge, for the entire time of flight. Adoption of a normalized time domain requires the development of new equations for the sweep method, which yields all the time-varying gain matrices, calculated offline and stored onboard. In this mathematical framework, the updating formula for the time of flight and the guidance termination criterion are derived in a logical, consistent fashion. VTD-NOG identifies the trajectory corrections by assuming a thrust direction always aligned with the longitudinal axis of the spacecraft. However, this assumption represents an approximation, and the attitude

control system must be capable of maintaining the actual spacecraft orientation sufficiently close to this thrust alignment condition. To do this, the attitude control system uses thrust vector control (TVC). This technique is widely employed for rocket and spacecraft attitude control (Tewari 2011). PD control represents a consolidated approach to designing a closed-loop attitude control system (Greensite 1970). However, plain PD control can lead to excessive angular rates for the thrust deflection. In fact, high proportional and derivative gains are often needed to obtain a fast response of the attitude control loop. Thus, in this work, attitude control is performed using CPD, which introduces an appropriate saturation action, with the final aim of maintaining the angular rates within acceptable limits.

This research has thus the ultimate purpose of demonstrating that the joint use of VTD-NOG and CPD indeed represents an effective methodology for spacecraft guidance and control, with special reference to lunar ascent path and accurate orbit injection, in the presence of nonnominal flight conditions. A preliminary version of this study can be found in Pontani and Celani 2017.

NOMINAL TRAJECTORY

This research treats the problem of driving a space vehicle from the Moon surface to a final elliptic orbit, with given perilune and apolune altitudes (denoted respectively with h_P and h_A; $h_P = 15$ km and $h_A = 100$ km), in the presence of nonnominal flight conditions. Both trajectory and attitude dynamics of the space vehicle are modeled. This section is specifically focused on defining the nominal ascent path. In this context, the spacecraft is modeled as a point mass (denoted with S in Figure 1). Subsequently, attitude dynamics is considered, with the final aim of determining the appropriate thrust vector control action.

The nominal vehicle ascent path is assumed to end at periselenium, and is investigated under the following three assumptions: (i) the Moon and its mass distribution are spherical, (ii) the Moon does not rotate, and (iii) the vehicle thrust is continuous and has constant magnitude. While (i) and (ii) are reasonable approximations, due to the short time of flight, assumption (iii) implies that the thrust acceleration $\left(T/\tilde{m}\right)$ is

$$\frac{T}{\tilde{m}} = \frac{n_0 c}{c - n_0 t} \tag{1}$$

where c is the (constant) effective ejection velocity of the propulsive system, n_0 is the initial thrust acceleration (at t_0, set to 0), and t is the actual time. The following nominal values are assumed: $n_0 = 0.25 g_0$ and $c = 3$ km/sec $\left(g_0 = 9.8 \text{ m/sec}^2\right)$.

Formulation of the problem

The spacecraft dynamics is described in a convenient Moon-centered inertial frame, identified by the right-handed sequence of unit vectors $\left(\hat{c}_1, \hat{c}_2, \hat{c}_3\right)$, where $\left(\hat{c}_1, \hat{c}_2\right)$ identifies the plane of the desired orbit and $\hat{c}_3$ is aligned with the related angular momentum. At the initial time the ascent vehicle is assumed to be placed at S_0, belonging to the plane of the desired orbit. In the problem formulation, both the Moon and its gravitational field are assumed spherical. As no additional external force affects the spacecraft motion and S_0 lies on the plane of the desired orbit (cf. Figure 1), the optimal ascent path can be sought in the $\left(\hat{c}_1, \hat{c}_2\right)$-plane. Such a coplanar trajectory can be conjectured to outperform any alternative three-dimensional path. In fact, due to symmetry of the gravitational field, any out-of-plane thrust maneuver would imply a useless waste of propellant, with the only effect of adding a non-coplanar component to the instantaneous velocity. In the $\left(\hat{c}_1, \hat{c}_2\right)$-plane, the time-varying position of the space vehicle can be identified by the following two variables: radius r and right ascension ξ, illustrated in Figure 1. The spacecraft velocity can be projected along the two axes $\left(\hat{r}, \hat{t}\right)$, where $\hat{r}$ points toward the position vector $\boldsymbol{r}$ and $\hat{t}$ is in the direction of the spacecraft motion (cf. Figure 1). The related components are denoted with $\left(v_r, v_t\right)$ and termed radial and transverse velocity component, respectively.

The state vector consists of the two components of the position and velocity vectors, and is given by $\boldsymbol{x} := \begin{bmatrix} x_1 & x_2 & x_3 & x_4 \end{bmatrix}^T = \begin{bmatrix} r & \xi & v_r & v_t \end{bmatrix}^T$. The spacecraft is controlled through the thrust direction $\hat{T}$, defined by the angle α (cf. Figure 1). Thus, the control vector $\boldsymbol{u}$ is $\boldsymbol{u} := \alpha$.

The dynamics equations, also termed state equations henceforth, describe the spacecraft motion, and involve both the state and the control vectors,

$$\dot{r} = v_r \qquad \dot{\xi} = \frac{v_t}{r} \qquad \dot{v}_r = -\frac{\mu}{r^2} + \frac{v_t^2}{r} + \frac{T}{\tilde{m}}\sin\alpha \qquad \dot{v}_t = \frac{-v_t v_r}{r} + \frac{T}{\tilde{m}}\cos\alpha \tag{2}$$

where $(T/\tilde{m})$ is given by Eq. (1) and μ $\left(=4902.9\ \mathrm{km}^3/\mathrm{sec}^2\right)$ is the Moon gravitational parameter. This work uses the two variables (v_r, v_t) in place of the more usual set formed by (γ, v), i.e. velocity magnitude *v* and flight path angle γ. This choice allows avoiding singularities in the equations of motion, because the velocity magnitude equals zero at liftoff from the Moon surface. Equations (2) can be written in the compact form

$$\dot{\boldsymbol{x}} = \tilde{\boldsymbol{f}}(\boldsymbol{x}, \boldsymbol{u}, t) \tag{3}$$

Due to the definition of the inertial frame in relation to the initial spacecraft position, the initial conditions (denoted with the subscript "0") are

$$r_0 = R_M \qquad \xi_0 = 0 \qquad v_{r0} = 0 \qquad v_{t0} = 0 \tag{4}$$

where R_M $(=1738\ \mathrm{km})$ is the Moon radius. The final conditions (denoted with the subscript "f") at orbit injection are

$$r_f = R_M + h_P \qquad v_{rf} = 0 \qquad v_{tf} = \sqrt{\frac{\mu}{a}\frac{1+e}{1-e}} \tag{5}$$

where *e* and *a* are respectivley the eccentricity and the semimajor axis of the desired orbit. Equations (4)-(5) can be written in compact form as

$$\boldsymbol{\psi}\left(\boldsymbol{x}_0, \boldsymbol{x}_f, t_f\right) = \boldsymbol{0} \tag{6}$$

The problem of interest can be reformulated by using the dimensionless (normalized) time τ,

$$\tau := t/t_f \qquad \Rightarrow \qquad \tau_0 \equiv 0 \le \tau \le 1 \equiv \tau_f \tag{7}$$

Let the dot denote the derivative with respect to τ henceforth. Equations (3) are rewritten as

$$\dot{\boldsymbol{x}} = t_f \tilde{\boldsymbol{f}}\left(\boldsymbol{x}, \boldsymbol{u}, t_f \tau\right) =: \boldsymbol{f}\left(\boldsymbol{x}, \boldsymbol{u}, \boldsymbol{a}, \tau\right) \tag{8}$$

where $\boldsymbol{a}$ collects all the unknown parameters of the problem ($\boldsymbol{a} = t_f$ for the problem at hand).

Due to assumption (iii), minimizing the time of flight $\left(t_f - t_0\right)$ is equivalent to minimizing the propellant consumption. Thus, as t_0 is set to 0, the objective function is

$$J = t_f \tag{9}$$

First-order conditions for optimal thrust programming

In order to obtain the necessary conditions for a minimizing (optimal) solution, a Hamiltonian H and a boundary condition function Φ are introduced as

$$H(\boldsymbol{x},\boldsymbol{u},\boldsymbol{a}) := \boldsymbol{\lambda}^T \boldsymbol{f} = \lambda_1 t_f x_3 + \lambda_2 \frac{t_f x_4}{x_1} + \lambda_3 t_f \left[-\frac{\mu}{x_1^2} + \frac{x_4^2}{x_1} + \frac{T}{\tilde{m}} \sin u_1 \right] + \lambda_4 t_f \left[\frac{-x_3 x_4}{x_1} + \frac{T}{\tilde{m}} \cos u_1 \right] \tag{10}$$

$$\begin{aligned} \Phi(\boldsymbol{x}_0, \boldsymbol{x}_f, \boldsymbol{a}) := J + \boldsymbol{\upsilon}^T \boldsymbol{\psi} = t_f + \upsilon_1 (x_{10} - R_M) + \upsilon_2 x_{20} + \upsilon_3 x_{30} + \upsilon_4 x_{40} \\ + \upsilon_5 \left[x_{1f} - (R_M + h_P) \right] + \upsilon_6 x_{3f} + \upsilon_7 \left[x_{4f} - \sqrt{\frac{\mu}{a} \frac{1+e}{1-e}} \right] \end{aligned} \tag{11}$$

where $x_{k0} = x_k(\tau_0)$ and $x_{kf} = x_k(\tau_f)$ $(k = 1,\ldots,4)$; $\boldsymbol{\lambda} \left(:= [\lambda_1 \quad \lambda_2 \quad \lambda_3 \quad \lambda_4]^T\right)$ and $\boldsymbol{\upsilon} \left(:= [\upsilon_1 \quad \upsilon_2 \quad \upsilon_3 \quad \upsilon_4 \quad \upsilon_5 \quad \upsilon_6 \quad \upsilon_7]^T\right)$ denote respectively the adjoint variable conjugate to the equations of motion (2) and to the boundary conditions (4)-(5).

The first-order necessary conditions for (local) optimality (cf. Hull 2003) include the costate (or adjoint) equations, in conjunction with the respective boundary conditions,

$$\dot{\boldsymbol{\lambda}} = -\left[\frac{\partial H}{\partial \boldsymbol{x}} \right]^T \qquad \boldsymbol{\lambda}_0 = -\left[\frac{\partial \Phi}{\partial \boldsymbol{x}_0} \right]^T \qquad \boldsymbol{\lambda}_f = \left[\frac{\partial \Phi}{\partial \boldsymbol{x}_f} \right]^T \tag{12}$$

leading to $\lambda_2 = 0 \ \forall \tau$. The scalar expressions of the adjoint equations are not reported for the sake of brevity. The Pontryagin minimum principle allows expressing the optimal control $\boldsymbol{u}^*$ in terms of the costates,

$$\boldsymbol{u}^* = \arg\min_{\boldsymbol{u}} H = \arg\min_{\boldsymbol{u}} \left\{ \frac{T}{\tilde{m}} t_f \left(\lambda_3 \sin u_1 + \lambda_4 \cos u_1 \right) \right\}$$

The right-hand side can be written as a dot product,

$$\boldsymbol{u}^* = \arg\min_{\boldsymbol{u}} \left\{ \frac{T}{\tilde{m}} t_f \left[\sin u_1 \quad \cos u_1 \right] \left[\lambda_3 \quad \lambda_4 \right]^T \right\}$$

The latter relation leads to obtaining the optimal control angle α^*,

$$\sin\alpha^* = \sin u_1^* = -\frac{\lambda_3^*}{\sqrt{\lambda_3^{*2} + \lambda_4^{*2}}} \quad \text{and} \quad \cos\alpha^* = \cos u_1^* = -\frac{\lambda_4^*}{\sqrt{\lambda_3^{*2} + \lambda_4^{*2}}} \tag{13}$$

It is worth remarking that the Pontryagin minimum implies satisfaction of both the first-order stationarity condition, i.e. $H_{\boldsymbol{u}}^* = \mathbf{0}^T$, and the second-order (necessary) condition on positive semidefiniteness of the Hessian $H_{\boldsymbol{uu}}^*$. The latter condition is specifically dealt with in the next subsection, focused on second-order conditions for optimality. Lastly, the parameter condition (cf. Hull 2003) must hold, and yields

$$\int_0^1 \left[\frac{\partial H}{\partial \boldsymbol{a}}\right]^T d\tau + \left[\frac{\partial \Phi}{\partial \boldsymbol{a}}\right]^T = \mathbf{0} \quad \Rightarrow \quad \int_0^1 \boldsymbol{\lambda}^T \frac{\partial \boldsymbol{f}}{\partial t_f} d\tau + 1 = 0 \tag{14}$$

After introducing the additional variable $\boldsymbol{\mu}$, Eq. (14) is equivalent to

$$\dot{\boldsymbol{\mu}} = -\left[\frac{\partial H}{\partial \boldsymbol{a}}\right]^T \quad \text{with} \quad \boldsymbol{\mu}_0 = \mathbf{0} \quad \text{and} \quad \boldsymbol{\mu}_f - \left[\frac{\partial \Phi}{\partial \boldsymbol{a}}\right]^T = \mathbf{0} \tag{15}$$

Through the necessary conditions for optimality, the optimal control problem is translated into a two-point boundary-value problem, with unknowns represented by t_f and the initial values of $\boldsymbol{\lambda}$.

However, the parameter condition (14) can be transformed into an inequality constraint, as a consequence of homogeneity of the costate equations, in conjunction with Eq. (13), in which the control angle is expressed as the ratio of adjoint variables. In fact, due to Eq. (13), homogeneity implies that if $\boldsymbol{\lambda}$ is proportional to $\boldsymbol{\lambda}^*$ ($\boldsymbol{\lambda} = k_\lambda \boldsymbol{\lambda}^*$; k_λ denotes a positive constant), then the final conditions (5) are fulfilled at τ_f, while minimizing the time of flight. Instead, the parameter condition is not met, because the integral in Eq. (14) turns out to be

$$\int_0^1 \boldsymbol{\lambda}^T \frac{\partial \boldsymbol{f}}{\partial t_f} d\tau = k_\lambda \int_0^1 \boldsymbol{\lambda}^{*T} \frac{\partial \boldsymbol{f}}{\partial t_f} d\tau = -k_\lambda \neq -1 \tag{16}$$

Hence, if the proportionality condition is satisfied, then the optimal control $\boldsymbol{u}^*$ can be obtained without considering the parameter condition (14), which becomes ignorable as an equality constraint is replaced by the following inequality constraint:

$$\int_0^1 \boldsymbol{\lambda}^T \frac{\partial \boldsymbol{f}}{\partial t_f} d\tau < 0 \tag{17}$$

Moreover, $\lambda_2 = 0 \; \forall \tau$, as previously remarked, and the equation for x_2 is ignorable, because no dynamics equation includes the right ascension x_2 in the right-hand-side, and no final condition is specified for x_2. This circumstance implies that the optimal ascent path optimization problem can be formulated as a two-point boundary-value problem, involving the initial values of the adjoint variables (λ_1, λ_3, and λ_4) and the time of flight t_f as unknowns.

Second-order conditions for optimal thrust programming

The second-order optimality conditions refer to a neighboring optimal comparison path, which can lie in the proximity of the optimal trajectory, and satisfies to first order the state and the adjoint equations, together with the related boundary conditions. With reference to a candidate optimal solution, associated with the state $\boldsymbol{x}^*$, costate $\boldsymbol{\lambda}^*$ and control $\boldsymbol{u}^*$, optimality is guaranteed if no neighboring optimal path exists.

The first second-order condition is the *Clebsch-Legendre sufficient condition* for a minimum (cf. Hull 2003), i.e. $H^*_{\boldsymbol{uu}} > 0$. In the necessary form the sign "$\geq$" replaces the inequality sign (i.e. the Hessian $H^*_{\boldsymbol{uu}}$ must be positive semidefinite).

In general, a neighboring optimal trajectory satisfies both the state equations and the boundary conditions to first order. This means that the state and costate displacements ($\delta\boldsymbol{x}, \delta\boldsymbol{\lambda}$) satisfy the linear equations deriving from Eqs. (8) and (12),

$$\delta\dot{\boldsymbol{x}} = \boldsymbol{f}_{\boldsymbol{x}}\delta\boldsymbol{x} + \boldsymbol{f}_{\boldsymbol{u}}\delta\boldsymbol{u} + \boldsymbol{f}_{\boldsymbol{a}}d\boldsymbol{a} \qquad \delta\dot{\boldsymbol{\lambda}} = -H_{\boldsymbol{xx}}\delta\boldsymbol{x} - H_{\boldsymbol{xu}}\delta\boldsymbol{u} - H_{\boldsymbol{x\lambda}}\delta\boldsymbol{\lambda} - H_{\boldsymbol{xa}}d\boldsymbol{a} \tag{18}$$

while the fact that the Hamiltonian is stationary with respect to $\boldsymbol{u}$, i.e. $H^*_{\boldsymbol{u}} = \boldsymbol{0}^T$, yields

$$H_{\boldsymbol{ux}}\delta\boldsymbol{x} + H_{\boldsymbol{uu}}\delta\boldsymbol{u} + H_{\boldsymbol{ua}}d\boldsymbol{a} + H_{\boldsymbol{u\lambda}}\delta\boldsymbol{\lambda} = \boldsymbol{0} \tag{19}$$

The boundary conditions for Eqs. (19) are derived from Eqs. (6) and (12),

$$\boldsymbol{\psi}_{\boldsymbol{x}_f}\delta\boldsymbol{x}_f + \boldsymbol{\psi}_{\boldsymbol{x}_0}\delta\boldsymbol{x}_0 + \boldsymbol{\psi}_{\boldsymbol{a}}d\boldsymbol{a} = \boldsymbol{0} \tag{20}$$

$$\delta\boldsymbol{\lambda}_0 = -\Phi_{\boldsymbol{x}_0\boldsymbol{x}_0}\delta\boldsymbol{x}_0 - \Phi_{\boldsymbol{x}_0\boldsymbol{a}}d\boldsymbol{a} - \boldsymbol{\psi}^T_{\boldsymbol{x}_0}d\boldsymbol{v} \qquad \delta\boldsymbol{\lambda}_f = \Phi_{\boldsymbol{x}_f\boldsymbol{x}_f}\delta\boldsymbol{x}_f + \Phi_{\boldsymbol{x}_f\boldsymbol{a}}d\boldsymbol{a} + \boldsymbol{\psi}^T_{\boldsymbol{x}_f}d\boldsymbol{v} \tag{21}$$

where Eqs. (21) are written under the assumption that $\Phi_{x_0 x_f} = \Phi_{x_f x_0} = 0$, condition that is fulfilled for the problem at hand. Equation (15) replaces the remaining parameter condition (14), and leads to the following relations:

$$\delta\dot{\boldsymbol{\mu}} = -H_{\boldsymbol{ax}}\delta\boldsymbol{x} - H_{\boldsymbol{au}}\delta\boldsymbol{u} - H_{\boldsymbol{aa}}\delta\boldsymbol{a} - H_{\boldsymbol{a\lambda}}\delta\boldsymbol{\lambda}, \quad \text{with} \quad \delta\boldsymbol{\mu}_0 = \mathbf{0}, \qquad \delta\boldsymbol{\mu}_f - \Phi_{\boldsymbol{ax}_f}\delta\boldsymbol{x}_f - \Phi_{\boldsymbol{aa}}\delta\boldsymbol{a}^T - \boldsymbol{\psi}_{\boldsymbol{a}}^T d\boldsymbol{v} = \mathbf{0} \tag{22}$$

where Eq. (22) is written under the assumption that $\Phi_{\boldsymbol{ax}_0} = 0$, condition that is fulfilled again for the problem of interest. Under the assumption that the Clebsch-Legendre condition holds, Eq. (19) can be solved for $\delta\boldsymbol{u}$,

$$\delta\boldsymbol{u} = -H_{\boldsymbol{uu}}^{-1}\left(H_{\boldsymbol{ux}}\delta\boldsymbol{x} + H_{\boldsymbol{ua}}d\boldsymbol{a} + H_{\boldsymbol{u\lambda}}\delta\boldsymbol{\lambda}\right) \tag{23}$$

After inserting Eq. (25) in Eqs. (18) and (22), one obtains

$$\delta\dot{\boldsymbol{x}} = \mathbf{A}\delta\boldsymbol{x} - \mathbf{B}\delta\boldsymbol{\lambda} + \mathbf{D}d\boldsymbol{a}, \quad \delta\dot{\boldsymbol{\lambda}} = -\mathbf{C}\delta\boldsymbol{x} - \mathbf{A}^T\delta\boldsymbol{\lambda} - \mathbf{E}d\boldsymbol{a}, \quad \delta\dot{\boldsymbol{\mu}} = -\mathbf{E}^T\delta\boldsymbol{x} - \mathbf{D}^T\delta\boldsymbol{\lambda} - \mathbf{F}d\boldsymbol{a} \tag{24}$$

where the matrices **A**, **B**, **C**, **D**, **E**, and **F** depend on the quantities appearing in Eqs. (18), (19), and (22); their expressions are not reported for the sake of brevity. The final conditions in Eqs. (20), (21), and (22) motivate the definition of the sweep variables,

$$\delta\boldsymbol{\lambda} = \mathbf{S}\delta\boldsymbol{x} + \mathbf{R}d\boldsymbol{v} + \mathbf{m}d\boldsymbol{a}, \quad \mathbf{0} = \mathbf{R}^T\delta\boldsymbol{x} + \mathbf{Q}d\boldsymbol{v} + \mathbf{n}d\boldsymbol{a}, \quad \delta\boldsymbol{\mu} = \mathbf{m}^T\delta\boldsymbol{x} + \mathbf{n}^T d\boldsymbol{v} + \boldsymbol{\alpha}d\boldsymbol{a} \tag{25}$$

Matrices **S**, **R**, **m**, **Q**, **n**, and $\boldsymbol{\alpha}$ fulfill the sweep equations, derived in Hull 2003 and not reported in this work for the sake of conciseness. The second and the third equation contained in Eq. (25) can be solved simultaneously at τ_0 (at which $\delta\boldsymbol{\mu}_0 = \mathbf{0}$, cf. Eq. (22)), to yield

$$\begin{bmatrix} d\boldsymbol{v} \\ d\boldsymbol{a} \end{bmatrix} = -\mathbf{V}_0^{-1}\mathbf{U}_0^T\delta\boldsymbol{x}_0, \quad \text{where} \quad \mathbf{U} := \begin{bmatrix} \mathbf{R} & \mathbf{m} \end{bmatrix} \quad \text{and} \quad \mathbf{V} := \begin{bmatrix} \mathbf{Q} & \mathbf{n} \\ \mathbf{n}^T & \boldsymbol{\alpha} \end{bmatrix} \tag{26}$$

If Eq. (26) is used at τ_0, then $\delta\boldsymbol{\lambda}_0 = \left(\mathbf{S}_0 - \mathbf{U}_0\mathbf{V}_0^{-1}\mathbf{U}_0^T\right)\delta\boldsymbol{x}_0$. Letting $\hat{\mathbf{S}} := \mathbf{S} - \mathbf{U}\mathbf{V}^{-1}\mathbf{U}^T$, it is relatively straightforward to prove that the same sweep equation satisfied by **S** must hold also for $\hat{\mathbf{S}}$ (with $\hat{\mathbf{S}}$ in place of **S**), with boundary condition $\hat{\mathbf{S}} \to \infty$ as $\tau \to \tau_f \ (=1)$. From the previous relation on $\delta\boldsymbol{\lambda}_0$ and $\delta\boldsymbol{x}_0$ one can conclude that $\delta\boldsymbol{\lambda}_0 \to \mathbf{0}$ as $\delta\boldsymbol{x}_0 \to \mathbf{0}$, unless $\hat{\mathbf{S}}$ tends to infinity at an internal time $\bar{\tau}$ $\left(\tau_0 \le \bar{\tau} < \tau_f\right)$, which is

209 referred to as conjugate point. In the end, if $\hat{\mathbf{S}} < \infty \ \ \forall \tau \in \left[\tau_0, \tau_f \right[$, then no conjugate point exists and, as a
210 consequence, no neighboring optimal solution exists.
211
212 **Optimal ascent trajectory**
213 This subsection addresses the numerical determination of the minimum-time ascent path leading to injection
214 into the desired lunar orbit.
215 The determination of optimal (either minimum propellant consumption or minimum time) space trajectories
216 has been pursued with several numerical methods, for decades. Classical optimization approaches are usually
217 classified as (i) indirect methods and (ii) direct techniques. The former approaches are based on applying the
218 necessary conditions for optimality (i.e. the Euler-Lagrange equations and the Pontryagin minimum principle),
219 which arise from the calculus of variations (Miele and Wang 1997, Miele and Mancuso 2001). Direct algorithms
220 convert the optimal control problem into a nonlinear programming problem (usually involving many
221 parameters). This class of methods includes direct transcription (Enright and Conway 1992), direct collocation
222 with nonlinear programming (Enright and Conway 1991), and differential inclusion (Seywald 1994). Due to
223 their theoretical foundations, direct and indirect algorithms possess specific features, which are investigated
224 thouroughly in the scientific literature (Betts 1998, Conway 2012). The two main limitations of classical
225 methods are (a) the need of a starting guess and (b) the locality of the results.
226 These disadvantages have motivated the introduction of heuristic techniques, which use a population of
227 individuals, associated with possible solutions to the problem of interest. The initial population is generated
228 randomly, and therefore no guess is to be supplied. The optimal solution is sought through competition and
229 cooperation among individuals. As a preliminary step, for the purpose of applying a heuristic technique, optimal
230 control problems must be converted into parameter optimization problems. The lack of any analytical proof on
231 convergence of a heuristic method (even to a locally minimizing solution) represents their main disadvatage.
232 Furthermore, if a specific functional form is employed for the control variables, a heuristic method can find at
233 most the best solution in the class of functions used in the numerical solution process.

In this research, the first-order conditions for optimality are used, in conjunction with a simple implementation of particle swarm algorithm (PSO), which is extremely intuitive and easy-to-implement. More specifically, the necessary conditions for optimality are used to express the control variables in terms of the adjoint variables, which obey the costate equations (accompanied by the related boundary conditions). As a result, a reduced parameter set suffices to transcribe the optimal control problem into a parameter optimization problem. Moreover, satisfaction of all the necessary conditions guarantees (at least the local) optimality of the solution. This methodology, termed indirect heuristic algorithm, is thus capable of avoiding the main disadvantages of using heuristic approaches, while retaining the main advantage, which is the absence of any starting guess. In the scientific literature (Pontani and Conway 2010, Pontani et al. 2012, Pontani and Conway 2013, Pontani and Conway 2012, and Pontani and Conway 2014) several papers employ successfully PSO for solving trajectory optimization problems.

In this work, the parameter set includes $\{\lambda_{10}, \lambda_{30}, \lambda_{40}, t_f\}$. The boundary conditions are represented by the three equalities reported in Eq. (5), accompanied by the inequality (17). Once the optimal parameter set has been found, the (two-dimensional) state and adjoint equations can be integrated, using Eq. (13) to express the control angle α as a function of the costate variables.

For the problem of interest the swarming algorithm uses 100 particles and is run for 500 iterations. A set of canonical units is adopted: the Moon radius is the distance unit $(1\ \mathrm{DU} = 1738\ \mathrm{km})$, whereas the time unit is such that $\mu = 1\ \mathrm{DU}^3/\mathrm{TU}^2$ (i.e. $1\ \mathrm{TU} = 1034.8\ \mathrm{sec}$). The search space is defined by the inequalities $-1 \le \lambda_{k0} \le 1 \quad (k = 1,3,4)$ and $0.5\ \mathrm{TU} \le t_f \le 3\ \mathrm{TU}$. It is worth noticing that the adjoint variables can be sought in an arbitrary interval, because of ignorability of the parameter condition. The PSO algorithm is able to obtain the optimal (two-dimensional) ascent trajectory with great accuracy. In fact, the errors on the final conditions are $\left| r_f^* - (R_M + h_P) \right| = 1.158 \cdot 10^{-12}$ km , $\left| v_{rf}^* \right| = 3.152 \cdot 10^{-15}$ km/sec , and $\left| v_{tf}^* - \sqrt{\frac{\mu}{a}\frac{1+e}{1-e}} \right| = 3.356 \cdot 10^{-15}$ km/sec , whereas the minimum time is $t_f^* = 9.576$ min . Figure 2 and Figure 3 portray the state components corresponding to the optimal ascent path and the related optimal control angle time history.

The swarming algorithm employs the first-order necessary conditions to determine the optimal trajectory. However, the second-order sufficient conditions are also to be fulfilled so that the neighboring optimal guidance can be applied. Evaluation of the matrices H_{uu} and $\hat{\mathbf{S}}$ along the optimal path allows verifying that the second-order sufficient conditions for a minimum are both satisfied, and this represents the theoretical premise for a successful application of VTD-NOG.

VARIABLE-TIME-DOMAIN NEIGHBORING OPTIMAL GUIDANCE

The Variable-Time-Domain Neighboring optimal guidance (VTD-NOG) uses the minimum-time path as the reference trajectory, with the final aim of obtaining the control correction at each sampling time $\{t_k\}_{k=0,\ldots,n_S}$, with $t_0 = 0$. These are the times at which the state deviation of the actual path (associated with $\boldsymbol{x}$) from the nominal trajectory (corresponding to $\boldsymbol{x}^*$) is evaluated, to yield

$$d\boldsymbol{x}_k \equiv \delta\boldsymbol{x}_k = \boldsymbol{x}(t_k) - \boldsymbol{x}^*(t_k) \tag{27}$$

The total number of sampling times, n_S, is unspecified, whereas the actual time interval between two succeeding sampling times is prescribed and denoted with Δt_S, $\Delta t_S = t_{k+1} - t_k \quad (k = 0,\ldots,n_S - 1)$. It is apparent that an essential ingredient for implementing VTD-NOG is the formula for the determination of $t_f^{(k)}$, i.e. the overall time of flight computed at time t_k.

Time-to-go updating law and termination criterion

The basic principle that underlies the VTD-NOG algorithm consists in determining the control correction $\delta\boldsymbol{u}(\tau)$ in the generic interval $[\tau_k, \tau_{k+1}]$ such that the second differential of *J* is minimized (cf. Hull 2003), while holding the first-order expansions of the state equations, the related final conditions, and the parameter condition. Minimizing the second differential of *J* is equivalent to solving the accessory optimization problem, defined in the interval $[\tau_k, 1]$. Solving the same problem in the overall interval $[0,1]$ leads to deriving all the relations reported in the previous section (and in Hull 2003). This means that the latter relations need to be

extended to the generic interval $[\tau_k, 1]$. First, Eq. (18), the first and third relation of Eq. (22), Eq. (20), and the second relation of Eq. (21) as well as Eq. (19) remain unchanged. The latter yields the control correction,

$$\delta \boldsymbol{u} = -H_{uu}^{-1}\left(H_{ux}\delta \boldsymbol{x} + H_{ua} d\boldsymbol{a} + H_{u\lambda}\delta \boldsymbol{\lambda}\right) \qquad \tau_k \le \tau \le \tau_{k+1} \tag{28}$$

Equations (24) and the last two relations of Eqs. (25) can be derived again, through the same steps described in Hull 2003, but they are not reported for the sake of brevity. However, Eq. (26), which derives from the last two relations of Eqs. (25), is now to be evaluated at τ_k,

$$\begin{bmatrix} d\boldsymbol{v} \\ d\boldsymbol{a} \end{bmatrix} = -\mathbf{V}_k^{-1}\mathbf{U}_k^T \delta \boldsymbol{x}_k - \mathbf{V}_k^{-1}\boldsymbol{\Theta}\delta \boldsymbol{\mu}_k \qquad \text{with} \qquad \boldsymbol{\Theta} := \begin{bmatrix} \mathbf{0}_{qxp} \\ \mathbf{I}_{pxp} \end{bmatrix} \tag{29}$$

because $\delta \boldsymbol{\mu}_k \neq \mathbf{0}$ (unlike $\delta \boldsymbol{\mu}_0 = \mathbf{0}$). The latter relation supplies the corrections $d\boldsymbol{v}$ and $d\boldsymbol{a}$ at τ_k as functions of the gain matrices **U** and **V**, $\delta \boldsymbol{x}_k$, and $\delta \boldsymbol{\mu}_k$ (coming from the numerical integration of the last of Eq. (24) in the previous interval $[\tau_{k-1}, \tau_k]$). Actually, Eq. (29) includes the updating law of the flight time t_f, which is a component of $\boldsymbol{a}$. Hence, if $dt_f^{(k)}$ denotes the correction on t_f^* evaluated at τ_k, then $t_f^{(k)} = t_f^* + dt_f^{(k)}$. Because the actual sampling interval Δt_S is specified, the general formula for τ_k is

$$\tau_{k+1} = \sum_{j=0}^{k} \frac{\Delta t_S}{t_f^{(j)}} \qquad \left(k = 0, \ldots, n_S - 1;\ t_f^{(0)} = t_f^*\right) \tag{30}$$

The total number of intervals n_S is found at the first occurrence of the following condition:

$$\sum_{j=0}^{n_S-1} \frac{\Delta t_S}{t_f^{(j)}} \ge 1 \qquad \Rightarrow \qquad \tau_{n_S} = 1 \tag{31}$$

It is worth emphasizing that the updating formula for $t_f^{(k)}$ derives from the extension of the accessory optimization problem to the time interval $[\tau_k, 1]$. Moreover, the introduction of the normalized time τ has important implications. First, all the gain matrices are defined in the interval [0,1] and do not become singular. Second, the limiting values $\{\tau_k\}$ are evaluated at each sampling time by means of Eq. (30). Lastly, the termination criterion corresponds to the upper bound of the interval [0,1], to which τ is constrained.

Modified sweep method

The identification of a neighboring optimal solution requires the backward integration of the sweep equations. An appropriate integration methodology employs the classical sweep equations for **S** in the interval $[\tau_{sw},1]$ (where τ_{sw} is sufficiently close to $\tau_f = 1$), and then switches to $\hat{\mathbf{S}}$. However, due to Eq. (29), new relations are to be derived for $\hat{\mathbf{S}}$ and the related matrices.

First, after inserting Eq. (29) (evaluated at the generic τ) into the first of Eq. (25) one obtains

$$\delta\boldsymbol{\lambda} = \hat{\mathbf{S}}\delta\boldsymbol{x} - \mathbf{W}\delta\boldsymbol{\mu} \qquad \text{with} \qquad \mathbf{W} := \mathbf{U}\mathbf{V}^{-1}\boldsymbol{\Theta} \tag{32}$$

Due to the third of Eq. (25), the latter relation can be rewritten as

$$\delta\boldsymbol{\lambda} = \left(\hat{\mathbf{S}} - \mathbf{W}\mathbf{m}^T\right)\delta\boldsymbol{x} - \mathbf{W}\mathbf{n}^T d\upsilon - \mathbf{W}\boldsymbol{\alpha} d\boldsymbol{\alpha} \tag{33}$$

This relation replaces the first of Eq. (25).

Considerable analytical developments (described in Pontani et al. 2015a and Pontani et al. 2015b, and not reported in this work for the sake of conciseness) lead to the following modified sweep equations:

$$\dot{\hat{\mathbf{S}}} = -\hat{\mathbf{S}}\mathbf{A} + \hat{\mathbf{S}}\mathbf{B}\hat{\mathbf{S}} + \left[\hat{\mathbf{S}}\mathbf{D}\boldsymbol{\alpha}^{-1} + \mathbf{W}\mathbf{F}\boldsymbol{\alpha}^{-1} + \mathbf{E}\boldsymbol{\alpha}^{-1}\right]\mathbf{m}^T - \mathbf{W}\mathbf{E}^T - \mathbf{W}\mathbf{D}^T\hat{\mathbf{S}} - \mathbf{C} - \mathbf{A}^T\hat{\mathbf{S}} \qquad \dot{\mathbf{Q}} = -\mathbf{R}^T\mathbf{B}\mathbf{W}\mathbf{n}^T \tag{34}$$

$$\dot{\mathbf{R}}^T = \mathbf{R}^T\mathbf{B}\hat{\mathbf{S}} - \mathbf{R}^T\mathbf{A} - \mathbf{R}^T\mathbf{B}\mathbf{W}\mathbf{m}^T \qquad \dot{\mathbf{n}} = -\mathbf{R}^T\left(\mathbf{D} + \mathbf{B}\mathbf{W}\boldsymbol{\alpha}\right) \qquad \dot{\boldsymbol{\alpha}} = \mathbf{D}^T\mathbf{W}\boldsymbol{\alpha} - \mathbf{F} - \mathbf{m}^T\mathbf{B}\mathbf{W}\boldsymbol{\alpha} - \mathbf{m}^T\mathbf{D} \tag{35}$$

$$\dot{\mathbf{m}}^T = -\mathbf{m}^T\mathbf{A} + \mathbf{m}^T\mathbf{B}\hat{\mathbf{S}} - \mathbf{m}^T\mathbf{B}\mathbf{W}\mathbf{m}^T - \mathbf{E}^T - \mathbf{D}^T\hat{\mathbf{S}} + \mathbf{D}^T\mathbf{W}\mathbf{m}^T \tag{36}$$

In the end, the gain matrices **S**, $\hat{\mathbf{S}}$, **R**, **Q**, **n**, **m**, and $\boldsymbol{\alpha}$, can be integrated in two steps:

(a) the equations of the traditional sweep method (cf. Hull 2003), with the related boundary conditions are used in the interval $[\tau_{sw},1]$

(b) Equations (34)-(36) are used in the interval $[0,\tau_{sw}]$. The matrices **R**, **Q**, **n**, **m**, and $\boldsymbol{\alpha}$ are continuous across the switching time τ_{sw}, whereas $\hat{\mathbf{S}}$ is given by $\hat{\mathbf{S}} := \mathbf{S} - \mathbf{U}\mathbf{V}^{-1}\mathbf{U}^T$; in this work τ_{sw} is set to 0.99.

Preliminary offline computations and algorithm structure

The implementation of VTD-NOG requires several preliminary computations that can be performed offline. Then, the related results are stored onboard.

First of all, the optimal path must be found, together with the related state, costate, and control variables, which become the nominal ones. These are obtained in the time domain τ and are initially represented as sequences of equally-spaced values, e.g. $\boldsymbol{u}_i^* = \boldsymbol{u}^*(\tau_i)$ $\left(i = 0,\ldots,n_D;\ \tau_0 = 0 \text{ and } \tau_{n_D} = 1\right)$. However, in the presence of perturbations, VTD-NOG determines the control corrections $\delta\boldsymbol{u}(\tau)$ in each interval $[\tau_k, \tau_{k+1}]$, where the values $\{\tau_k\}$ do not coincide with the equally-spaced values $\{\tau_i\}$ associated with $\{\boldsymbol{u}_i^*\}$. Hence, interpolation is to be used for the control variable $\boldsymbol{u}^*$, so that the value of $\boldsymbol{u}^*$ can be evaluated at any arbitrary time in the interval $0 \le \tau \le 1$. Similarly, also the nominal state $\boldsymbol{x}^*$ and costate $\boldsymbol{\lambda}^*$ are to be interpolated. If a large number of points is selected ($n_D = 1000$ in this research), then piecewise linear interpolation is a suitable option and in fact is adopted in this work. The subsequent step consists in the analytical derivation of the matrices $\{\boldsymbol{f}_x, \boldsymbol{f}_u, \boldsymbol{f}_a, H_{xx}, H_{xu}, H_{x\lambda}, H_{xa}, H_{ux}, H_{uu}, H_{ua}, H_{u\lambda}, H_{ax}, H_{au}, H_{aa}, H_{a\lambda}, \psi_{x_f}, \psi_{x_0}, \psi_a, \Phi_{x_0x_0}, \Phi_{x_0a}, \Phi_{x_fx_f}, \Phi_{x_fa}, \Phi_{ax_f}, \Phi_{aa}\}$, which are evaluated along the optimal path. The matrices **A**, **B**, **C**, **D**, **E**, and **F** are introduced and evaluated, too. Then, the backward integration of the sweep equations is completed, and yields the matrices $\hat{\mathbf{S}}$, **R**, **m**, **Q**, **n**, and $\boldsymbol{\alpha}$. In this context, the analytic expressions of **W**, **U**, and **V** (written in terms of **R**, **m**, **Q**, **n**, and $\boldsymbol{\alpha}$) are used. All the remaining matrices (not yet interpolated) are interpolated as well, and this concludes the preliminary computations.

Using the nominal quantities (stored onboard), at each time τ_k the VTD-NOG algorithm determines the flight time $t_f^{(k)}$, the value τ_{k+1}, and the control correction $\delta\boldsymbol{u}(\tau)$. In particular, the following steps are needed in order to implement the guidance approach at hand:

1. Set the actual sampling time interval Δt_S
2. At each time τ_k $\left(k = 0,\ldots,n_S - 1;\ \tau_0 = 0\right)$

a. Evaluate $\delta \boldsymbol{x}_k$ thorugh Eq. (27)

b. Assume the value of $\delta \boldsymbol{\mu}$ calculated at the end of the preceding interval $\left[\tau_{k-1}, \tau_k\right]$ as $\delta \boldsymbol{\mu}_k$

c. Calculate the correction $dt_f^{(k)}$ and the updated time of flight $t_f^{(k)}$

d. Calculate the limiting value τ_{k+1}

e. Evaluate $\delta \boldsymbol{\lambda}_k$ and integrate the linear differential system composed of Eqs. (24)

f. Determine the control correction $\delta \boldsymbol{u}(\tau)$ in $\left[\tau_k, \tau_{k+1}\right]$ through Eq. (28)

3. If Eq. (31) holds, then VTD-NOG ends, otherwise point 2 is repeated (with *k* increased by 1).

Figure 4 depicts a block diagram that shows the sampled-data feedback structure of the VTD-NOG algorithm. The control and flight time corrections depend on the state deviation $\delta \boldsymbol{x}$ (evaluated at specified times) by means of the time-varying gain matrices. The attitude control loop (encircled by the dotted line) is being described in detail in the following.

CONSTRAINED PROPORTIONAL-DERIVATIVE ATTITUDE CONTROL

Thrust vectoring is used to control the attitude of the lunar module, through proper deflection of the engine. In this study, two-dimensional (nominal and perturbed) trajectories are considered, therefore the attitude is identified through only the pitch angle Θ (cf. Figure 5). The attitude equation governs pitch dynamics and is given by

$$I\ddot{\Theta} = Tl_c \sin\Delta \tag{37}$$

where *I* is the moment of inertia of the spacecraft about the y_b axis, l_c is the distance between the center of mass of the ascent module and the swivel point of the TVC, and Δ is the thrust deflection angle (cf. Figure 5).

The electro-hydraulic servoactuator that acts on the engine deflection angle is here modeled by the following first order system (Greensite 1970):

$$\dot{\tilde{\Delta}} = -\frac{1}{\tau_a}\tilde{\Delta} + \frac{1}{\tau_a}\Delta_c \tag{38}$$

In Eq. (38) Δ_c is the commanded deflection angle which represents the control input for the attitude control system, while the actual deflection Δ (appearing in Eq. (37)) is obtained by saturating $\tilde{\Delta}$ to the maximum deflection angle $\bar{\Delta}$,

$$\Delta = \mathrm{sat}_{\bar{\Delta}}\left(\tilde{\Delta}\right) = \begin{cases} -\bar{\Delta} & \text{if } \tilde{\Delta} < -\bar{\Delta} \\ \tilde{\Delta} & \text{if } -\bar{\Delta} \le \tilde{\Delta} \le \bar{\Delta} \\ \bar{\Delta} & \text{if } \tilde{\Delta} > \bar{\Delta} \end{cases} \tag{39}$$

The commanded pitch angle, denoted with Θ_c, is derived from the angle α provided by the VTD-NOG algorithm (cf. Figure 4). In fact, in the guidance algorithm the angle α is the desired (corrected) angle between $\hat{T}$ and $\hat{t}$, under the assumption that the thrust is aligned with the longitudinal axis of the spacecraft. Thus, α represents the desired angle between $\hat{x}_b$ and $\hat{t}$, and consequently the desired pitch angle is given by $\Theta_c = \alpha - \xi$. However, it is worth noticing that for simulating the spacecraft trajectory, the actual thrust angle $\alpha_a = \Theta + \xi - \Delta$ (cf. Figure 5) must be used in Eq. (2) in place of α.

A baseline attitude control action for such spacecraft is given by the following PD control:

$$\Delta_c = k_p\left(\Theta_c - \Theta\right) - k_d\dot{\Theta} \tag{40}$$

The variable $\dot{\Theta}_c$ is not continuous at sampling times, therefore including $\dot{\Theta}_c$ in Eq. (40) would result in large overshoots for Θ and large values for Δ and $\dot{\Delta}$ (cf. de Ruiter et al. 2013). It is worth noticing that most of the times Θ_c can be considered constant since the guidance commands usually change slowly compared to attitude maneuvers. If Θ_c is constant and the positive gains k_p and k_d satisfy $k_d > k_p\tau_a$, then the proposed PD control guarantees local convergence to the desired attitude (Greensite 1970). Moreover, in Celani 2018 it is shown that the control reported in Eq. (40) guarantees global convergence to the commanded attitude if the actuator dynamics is much faster than the attitude control loop. The considered PD control can lead to excessive angular rates for the thrust deflection. In fact, high values for the gains k_p and k_d might be required in order to obtain a fast response of the attitude control system in comparison with the guidance command. Then, high gains can in turn lead to high amplitudes for the rate of the TVC deflection angle. If the rates are too high then clearly they

become physically infeasible. The latter issue is here tackled by using Constrained Proportional and Derivative (CPD) control, which is described by the following equation:

$$\Delta_c = \mathrm{sat}_{\bar{\Delta}_c}\left(k_p\left(\Theta_c - \Theta\right) - k_d\dot{\Theta}\right) \tag{41}$$

where $\bar{\Delta}_c > 0$ is an additional design parameter. It will be shown next that employing CPD control ensures that

$$\left|\dot{\Delta}\right| \le \frac{2}{\tau_a}\bar{\Delta}_c \tag{42}$$

assuming that $\Delta(0) = 0$. Thus, an appropriate choice of $\bar{\Delta}_c$ guarantees that $\dot{\Delta}$ does not exceed physical limits. To show that Eq. (42) holds, first note that Eq. (38) and (41) imply

$$\left|\dot{\tilde{\Delta}}\right| \le \frac{1}{\tau_a}\left|\tilde{\Delta}\right| + \frac{1}{\tau_a}\bar{\Delta}_c \tag{43}$$

$$\dot{\tilde{\Delta}} \le -\frac{1}{\tau_a}\tilde{\Delta} + \frac{1}{\tau_a}\bar{\Delta}_c \qquad \text{and} \qquad -\dot{\tilde{\Delta}} \le \frac{1}{\tau_a}\tilde{\Delta} + \frac{1}{\tau_a}\bar{\Delta}_c \tag{44}$$

Thus, considering that $\tilde{\Delta}(0) = 0$ and using the Comparison Lemma (cf. Khalil 2000), it is easy to obtain that

$$\left|\tilde{\Delta}\right| \le \bar{\Delta}_c \tag{45}$$

Then, Eq. (42) follows directly from Eqs. (39), (43), and (45).

It is worth noticing that linearization of CPD control in Eq. (41) about $\Theta = \Theta_c$, $\dot{\Theta} = 0$ clearly reduces CPD to the standard PD control in Eq. (40). Thus, also CPD control achieves local convergence to the desired attitude.

Determination of control gains

The goal of the current subsection is presenting a method for determining at least first guess values for the gains k_p and k_d. Neglect dynamics of the actuator in Eq. (38) and linearize the closed-loop system in Eqs. (37) and (41) about $\Theta = \Theta_c$, $\dot{\Theta} = 0$, obtaining

$$I\ddot{\Theta} = Tl_c\left(k_p\left(\Theta_c - \Theta\right) - k_d\dot{\Theta}\right) \tag{46}$$

Thus, in the Laplace domain,

$$\frac{\hat{\Theta}(s)}{\hat{\Theta}_c(s)} = \frac{Gk_p}{s^2 + Gk_d s + Gk_p} \tag{47}$$

where $G = Tl_c / I$. Note that the value of G varies during the flight since so do the values of l_c and I. Let $\underline{G}$ and $\bar{G}$ be the minimum and maximum values of G along the considered flight. Then, the gains k_p and k_d are chosen so that for all $\underline{G} \le G \le \bar{G}$ it occurs that the transfer function in Eq. (46) possesses poles with damping ratio $\zeta \ge \underline{\zeta}$ and natural angular frequency $\omega_n \ge \underline{\omega}_n$. Magnitudes $\underline{\zeta}$ and $\underline{\omega}_n$ are chosen based on experience and proceeding by trial-and-error. Since $k_p G = \omega_n^2$ and $k_d G = 2\zeta\omega_n$, then it is easy to verify that specifications $\zeta \ge \underline{\zeta}$ and $\omega_n \ge \underline{\omega}_n$ are fulfilled for all $\underline{G} \le G \le \bar{G}$ by setting

$$k_p = \frac{\underline{\omega}_n^2}{\underline{G}} \qquad k_d = \frac{2\underline{\zeta}\underline{\omega}_n}{\underline{G}}\sqrt{\frac{\bar{G}}{\underline{G}}} \tag{48}$$

VTD-NOG & CPD APPLIED TO LUNAR ASCENT AND ORBIT INJECTION

The guidance and control methodology based on the joint use of VTD-NOG and CPD is applied to lunar ascent and orbit injection. The optimal ascent path is derived in a previous section and takes almost 10 minutes.

Further characteristics of the ascent vehicle are the initial mass $\tilde{m}_0$ $(= 4700 \text{ kg})$, the maximal deflection angle $\bar{\Delta}$ (set to 10 deg), and the time-varying distance l_c, given by $l_c = l_{c0} + \dot{l}_c t$, where $l_{c0} = 1$ m and $\dot{l}_c = 8.3 \cdot 10^{-4}$ m/sec. Usually, a (nominal) linear time history is also assumed for I, with initial and final values set respectively to $I_0 = 9200$ kg m^2 and $I_f = 4700$ kg m^2 for the problem at hand. These values are similar to those of the ascent module employed in the Apollo 11 mission. The value $\tau_a = 0.1$ sec is picked for the time constant of the electrohydraulic actuator.

Moreover, the following values are selected for VTD-NOG & CPD. The sampling interval Δt_S is set to 10 sec, and the CPD gains are determined as follows. First, note that the constant thrust equals $T = n_0 m_0$, the minimum value for l_c is given by $\underline{l_c} = l_{c0}$, and the maximum value for I is equal to $\bar{I} = I_0$. Moreover, the

maximum value of l_c can be set approximately to $\bar{l}_c = l_{c0} + \dot{l}_c t_f^* = 1.5$ m, whereas $\underline{I} = I_f = 4700$ kg m^2. Then, $\underline{G} = T\underline{l}_c / \bar{I} = 1.2514$ sec^{-2} and $\bar{G} = T\bar{l}_c / \underline{I} = 3.6744$ sec^{-2}. By inspection of the time behavior of Θ_c in nominal conditions, it seems appropriate picking $\underline{\omega}_n = 1$ rad/sec so to obtain an attitude control loop fast enough with respect to the speed of variation of nominal Θ_c. Moreover, proceeding by trial and error $\underline{\zeta}$ is set to 0.5. Thus, by Eq. (48) one obtains $k_p = 0.80$ and $k_d = 1.37$. In addition, the value 1.5 deg is selected for $\bar{\Delta}_c$ so that the inequality $|\dot{\Delta}| \le 30$ deg/sec is guaranteed (cf. Eq. (42)). Note that Eq. (45) implies that $|\tilde{\Delta}|$ is constrained to 1.5 deg. Thus, since $\bar{\Delta}$ = 10 deg, the same happens to the amplitude of Δ (cf. Eq. (39)).

The first reason for the existence of deviations from nominal flight conditions resides in the assumption that the thrust direction points toward the spacecraft longitudinal axis. This alignment condition was assumed for the derivation of the optimal ascent path. However, the actual spacecraft dynamics is driven by a thrust direction not exactly aligned with the longitudinal axis, due to the use of thrust vectoring for attitude control. This circumstance is apparent also by inspection of Figure 4, which illustrates clearly that the corrected control $\boldsymbol{u}$ does not coincide with the actual control $\boldsymbol{u}_a$, which affects the real dynamics of the center of mass. As a first step, VTD-NOG & CPD has been tested in order to evaluate these deviations, exclusively related to the alignment assumption. The first row of Table 1 (denoted with NC) reports the related results (obtained in a single simulation), i.e. the final displacements from the nominal final altitude and velocity components, and testifies to the excellent accuracy of VTD-NOG & CPD in this context.

However, perturbations can exist that affect the overall spacecraft dynamics. These can be related to the dynamical system itself or to environmental conditions. Monte Carlo (MC) campaigns are usually run, with the aim of attaining some statistical information on the accuracy of the guidance and control algorithm of interest, in the presence of the existing perturbations, which are simulated stochastically. In this research, propulsive perturbations are considered. In fact, the thrust magnitude (and the related acceleration) may exhibit modest (or moderate) fluctuations. This time-varying behavior is modeled through a trigonometric function with stochastic coefficients,

$$n_0^{(p)} = n_0\left[1+\sum_{k=1}^{5}\tilde{a}_k \sin\left(\frac{k\pi t}{t_f^*}\right)+\sum_{k=1}^{5}\tilde{a}_{k+5}\cos\left(\frac{k\pi t}{t_f^*}\right)\right] \tag{49}$$

where $n_0^{(p)}$ denotes the perturbed value of n_0, whereas the coefficients $\{\tilde{a}_k\}_{k=1,\ldots,10}$ have a random Gaussian distribution centered around the zero and a standard deviation equal to 0.02. It is worth remarking that oscillations of the thrust magnitude yield perturbed trajectories coplanar with the nominal path. Moreover, also the inertia moment may be subject to fluctuations, which make the actual time history nonlinear. These fluctuations are modeled again through trigonometric functions. Thus, the following time history is assumed for the inertia moment *I*:

$$I = \frac{I_f - I_0}{t_f^*}t + I_0 + \sum_{k=1}^{5}\tilde{b}_k \sin\left(\frac{k\pi t}{t_f^*}\right)+\sum_{k=1}^{5}\tilde{b}_{k+5}\left[\cos\left(\frac{k\pi t}{t_f^*}\right)-1\right] \tag{50}$$

In Eq. (50) the third and fourth terms represent the displacement from the nominal linear time history. The coefficients $\{\tilde{b}_k\}_{k=1,\ldots,10}$ are random quantities with uniform distribution in proper intervals such that the function (50) is nonincreasing in time. It is straightforward to recognize that a sufficient condition for monotonicity is

$$-\frac{I_0 - I_f}{10k\pi} \le \tilde{b}_k \le \frac{I_0 - I_f}{10k\pi} \tag{51}$$

Hence, in the Monte Carlo simulations, the random coefficients $\{\tilde{b}_k\}_{k=1,\ldots,10}$ are constrained to the interval specified in Eq. (51). At the end of VTD-NOG & CPD, the mean value and the standard deviation are evaluated, for all of the outputs of interest. The symbols $\overline{\Delta\chi}$ and $\chi^{(\sigma)}$ will denote the mean error (with respect to the nominal value) and standard deviation of χ henceforth.

Three Monte Carlo campaigns (MC) are performed: (i) MC1 assumes only nonlinearities for the time histories of the inertia moment *I*, (ii) MC2 considers thrust perturbations only, whereas (iii) MC3 assumes both deviations from nominal flight conditions. Each campaign includes 100 numerical simulations. With reference to MC3, Figure 6 and Figure 7 illustrate respectively the perturbed time histories $n_0^{(p)}$ and the time derivative of *I*, whereas Figure 8, Figure 9, Figure 10, Figure 11, Figure 12, and Figure 13 portray the time histories of the

relevant state variables, the commanded and actual pitch angle, as well as the engine deflection angle and its rate. All the state variables are subject to considerable deviations from the respective nominal time histories, as shown in Figure 8, Figure 9, and Figure 10. Nevertheless, inspection of Table 1, which reports the statistics on the errors at injection and the time of flight, reveals that VTD-NOG & CPD guarantees orbit injection with excellent accuracy, despite the relatively relaxed sampling time. Figure 11 and Figure 12 show that the deflection angle and the deflection rate do not exceed their respective maximal values. The commanded and the actual pitch angle, illustrated for a single perturbed path in Figure 13, are virtually indistinguishable after 15 seconds from liftoff. Furthermore, the average time of flight is very close to the nominal value, and the corresponding standard deviation is modest.

As a final remark, the runtime of VTD-NOG & CPD on an Intel i5-3570K @ 3.40 GHz takes 59 sec (while the nominal time of flight exceeds 9 minutes), and this guarantees that the guidance and control algorithm at hand can be implemented in real time.

CONCLUSION

This work proposes VTD-NOG & CPD, a new, general-purpose guidance and control algorithm for space vehicles, and describes its application to lunar ascent and orbit injection. VTD-NOG is a feedback guidance technique based on minimizing the second differential of the objective function. This minimization principle leads to deriving all the corrective maneuvers. A normalized time scale is adopted as the domain in which the nominal trajectory is defined. As a favorable consequence, the gain matrices remain finite for the entire time of flight, while the termination criterion and the updating law for the time of flight find consistent definitions. VTD-NOG identifies the trajectory corrections by assuming a thrust direction always aligned with the longitudinal axis of the spacecraft. CPD is employed for attitude control through TVC, and pursues this alignment condition. Unlike standard PD schemes, CPD introduces an appropriate saturation action, with the aim of maintaining the rate of the engine deflection angle within acceptable limits. Oscillations of the thrust magnitude and nonlinear variations of the inertia moment are assumed, and considerable deviations from the nominal flight conditions occur as a result, albeit the perturbed paths remain coplanar with the nominal

trajectory. VTD-NOG & CPD is thus applied to two-dimensional perturbed ascent paths, with the intent of ascertaining its effectiveness and accuracy. The Monte Carlo simulations performed in this study point out that orbit injection occurs with excellent accuracy, thus demonstrating that VTD-NOG & CPD indeed represents an effective methodology for the application at hand. Extension and testing of this guidance and control technique to perturbed three-dimensional trajectories, which may arise in the presence of supplementary deviations from nominal flight conditions, require more complete modeling of the attitude control system, as well as additional analytical developments, and represent the subject of further research.

REFERENCES

Afshari, H. H., Novinzadeh, A. B., and Roshanian, J. (2009). "Determination of Nonlinear Optimal Feedback Law for Satellite Injection Problem Using Neighboring Optimal Control." *Amer. J. Appl. Sciences*, 6(3), 430-438

Betts, J. T. (1998). "Survey of Numerical Methods for Trajectory Optimization." *J. Guid., Contr., and Dyn.*, 21, 193-207

Celani, F. (2018). "Global and Robust Attitude Control of a Launch Vehicle in Exoatmospheric Flight." *Aerosp. Sci. and Tech.*, 74, 22-36

Charalambous, C. B., Naidu, S. N., and Hibey, J. L. (1995). "Neighboring Optimal Trajectories for Aeroassisted Orbital Transfer Under Uncertainties." *J. Guid., Contr., and Dyn.*, 18(3), 478-485

Conway, B. A. (2012). "A Survey of Methods Available for the Numerical Optimization of Continuous Dynamic Systems." *J. Opt. Theory Appl.*, 152, 271-306

de Ruiter, A. H. J., Damaren, C. J., and Forbes, J. R. (2013). *Spacecraft dynamics and control: an introduction.* Wiley, Chichester, UK, 293

Enright, P. J. and Conway, B. A. (1991) "Optimal Finite-Thrust Spacecraft Trajectories Using Collocation and Nonlinear Programming." *J. Guid., Contr., and Dyn.*, 14, 981-985

Enright, P. J. and Conway, B. A. (1992) "Discrete Approximations to Optimal Trajectories Using Direct Transcription and Nonlinear Programming." *J. Guid., Contr., and Dyn.*, 15, 994-1002

Geller, D. K. (2006). "Linear Covariance Techniques for Orbital Rendezvous Analysis and Autonomous Onboard Mission Planning." *J. Guid., Contr., and Dyn.*, 29(6), 1404-1414

Greensite, A. L. (1970). *Analysis and design of space vehicle flight control systems. Control theory: Volume II*. Spartan Books, New York, NY, 175-192, 284-297

Hull, D. G. (2003). *Optimal Control Theory for Applications*. Springer International Edition, New York, NY, 199-254

Hull, D. G., and Nowak, M. J. (1993). "Neighboring Suboptimal Control for Vehicle Guidance." *Proc. AAS/AIAA Space Flight Conf.*, Pasadena, CA. Paper AAS 93-151

Khalil, H. K. (2000). *Nonlinear Systems*. Prentice Hall, Upper Saddle River, NJ, 102-103

Kugelmann, B. and Pesch, H. J. (1990a). "New General Guidance Method in Constrained Optimal Control, Part 1: Numerical Method." *J. Opt. Theory Appl.*, 67(3), 421-435

Kugelmann, B. and Pesch, H. J. (1990b). "New General Guidance Method in Constrained Optimal Control, Part 2: Application to Space Shuttle Guidance." *J. Opt. Theory Appl.*, 67(3), 437-446

Lam, Q. M., McFarland, M. B., Ruth, M., Drake, D., Ridgely, D. B., and Oppenheimer, M. W. (2008). "Adaptive Guidance and Control for Space Access Vehicle Subject to Control Surface Failures." *Proc. AIAA Guid., Nav. and Contr. Conf. and Exhibit*, Honolulu, HI. AIAA Paper 2008-7163

Lu, P. (1991). "Optimal Feedback Control Laws Using Nonlinear Programming." *J. Opt. Theory Appl.*, 71(3), 599-611

Marcos, A., Peñín, L. F., Sommer, J., and Bornschlegl, E. (2008). "Guidance and Control Design for the Ascent Phase of the Hopper RLV." *Proc. AIAA Guid., Nav. and Contr. Conf. and Exhibit*, Honolulu, HI. AIAA Paper 2008-7125

Miele, A. and Wang, T. (1997). "Optimal Trajectories for Earth-to-Mars Flight." *J. Opt. Theory Appl.*, 95(3), 467-499

Miele, A. and Mancuso, S. (2001). "Optimal Trajectories for Earth-Moon-Earth Flight." *A. Astron.*, 49(2), 59-71

Pontani, M. and Celani, F. (2017). "Neighboring Optimal Guidance and Attitude Control for Lunar Ascent and Orbit Injection." *Proc. 3rd IAA Conf. on Dyn. and Contr. of Space Syst.*, Moscow, Russian Federation

Pontani, M. and Conway, B. A. (2010). "Particle Swarm Optimization Applied to Space Trajectories." *J. Guid., Contr., and Dyn.*, 33(5), 1429-1441

Pontani, M., Ghosh, P., and Conway, B. A. (2012). "Particle Swarm Optimization of Multiple-Burn Rendezvous Trajectories." *J. Guid., Contr., and Dyn.*, 35(4), 1192-1207

Pontani, M. and Conway, B. A. (2013). "Optimal Finite-Thrust Rendezvous Trajectories Found via Particle Swarm Algorithm." *J. Spac. Rock.*, 50(6), 1222-1234

Pontani, M. and Conway, B. A. (2012). "Particle Swarm Optimization Applied to Impulsive Orbital Transfers." *A. Astron.*, 74, 141-155

Pontani, M. and Conway, B. A. (2014). "Optimal Low-Thrust Orbital Maneuvers via Indirect Swarming Method." *J. Opt. Theory Appl.*, 162(1), 272-292

Pontani, M., Cecchetti, G., and Teofilatto, P. (2015a). "Variable-Time-Domain Neighboring Optimal Guidance, Part 1: Algorithm Structure." *J. Opt. Theory Appl.*, 166(1), 76-92

Pontani, M., Cecchetti, G., and Teofilatto, P. (2015b). "Variable-time-domain neighboring optimal guidance applied to space trajectories." *A. Astron.*, 115, 102-120

Pontani, M., Cecchetti, G., and Teofilatto, P. (2015c). "Variable-Time-Domain Neighboring Optimal Guidance, Part 2: Application to Lunar Descent and Soft Landing." *J. Opt. Theory Appl.*, 166(1), 93-114

Pontani, M. (2016). "A New, General Neighboring Optimal Guidance for Aerospace Vehicles." *Variational Analysis and Aerospace Engineering.* Springer, New York, NY, Pasadena, CA, 421-449

Seywald, H. (1994). "Trajectory optimization Based on Differential Inclusion." *J. Guid., Contr., and Dyn.*, 17, 480-487

Seywald, H. and Cliff, E. M. (1994). "Neighboring Optimal Control Based Feedback Law for the Advanced Launch System." *J. Guid., Contr., and Dyn.*, 17(3), 1154-1162

Tian, B., Fan, W., and Zong, Q. (2015a). "Integrated Guidance and Control for Reusable Launch Vehicle in Reentry Phase." *Nonl. Dyn.*, 80(1-2), 397-412

Tian, B., Fan, W., Su, R. and Zong, Q. (2015b). "Real-time Trajectory and Attitude Coordination Control for Reusable Launch Vehicle in Reentry Phase." *IEEE Trans. Ind. Electron.*, 62(3), 1639-1650

Tewari, A. (2011). *Advanced Control of Aircraft, Spacecraft and Rockets*. Wiley, Chichester, UK, ch. 5

Yan, H., Fahroo, F., and Ross, I. M. (2002). "Real-Time Computation of Neighboring Optimal Control Laws." *Proc. AIAA Guid., Nav. and Contr. Conf. and Exhibit*, Monterey, CA. AIAA Paper 2002-4657

Yeh, F.-K. (2015). "Sliding-mode-based contour-following controller for guidance and autopilot systems of launch vehicles." *Proc. of the Inst. of Mech. Eng., Part G: J. of Aerosp. Eng.*, 227(2), 285-302

601

602 **TABLE 1.** Outputs using VTD-NOG & CPD
603

	$\overline{\Delta r_f}$	$\overline{\Delta v_{rf}}$	$\overline{\Delta v_{tf}}$	$\overline{t_f}$	$r_f^{(\sigma)}$	$v_{rf}^{(\sigma)}$	$v_{tf}^{(\sigma)}$	$t_f^{(\sigma)}$
NC	0.440	−0.199	−0.012	9.592	/	/	/	/
MC1	0.440	−0.197	−0.012	9.592	1.2e-4	3.0e-4	2.6e-5	5.3e-6
MC2	0.864	−0.041	0.108	9.590	2.604	0.605	2.662	0.145
MC3	1.203	−0.135	0.155	9.574	1.957	0.402	2.510	0.153

Legend. NC = nominal conditions, MC1 = Monte Carlo campaign with nonlinear inertia moment,
MC2 = Monte Carlo campaign with perturbed propulsion,
MC3 = Monte Carlo campaign with both deviations from nominal flight conditions.
Time in min, radius in m, velocity in m/sec. $\overline{t_f}$ = average time of flight

604

Figure 1

Click here to download Figure figure_01.eps

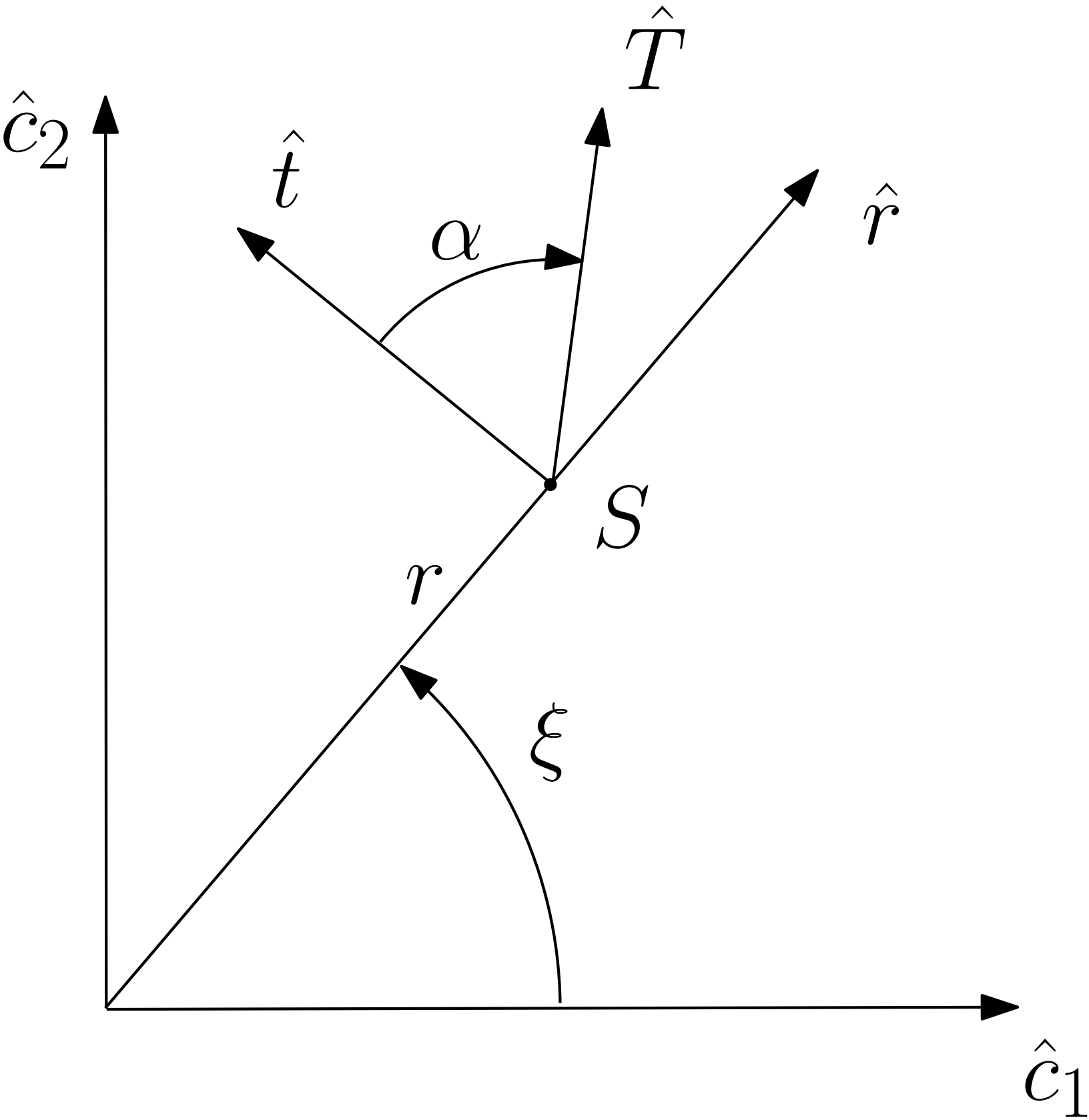

Figure 2

Click here to download Figure figure02.tif

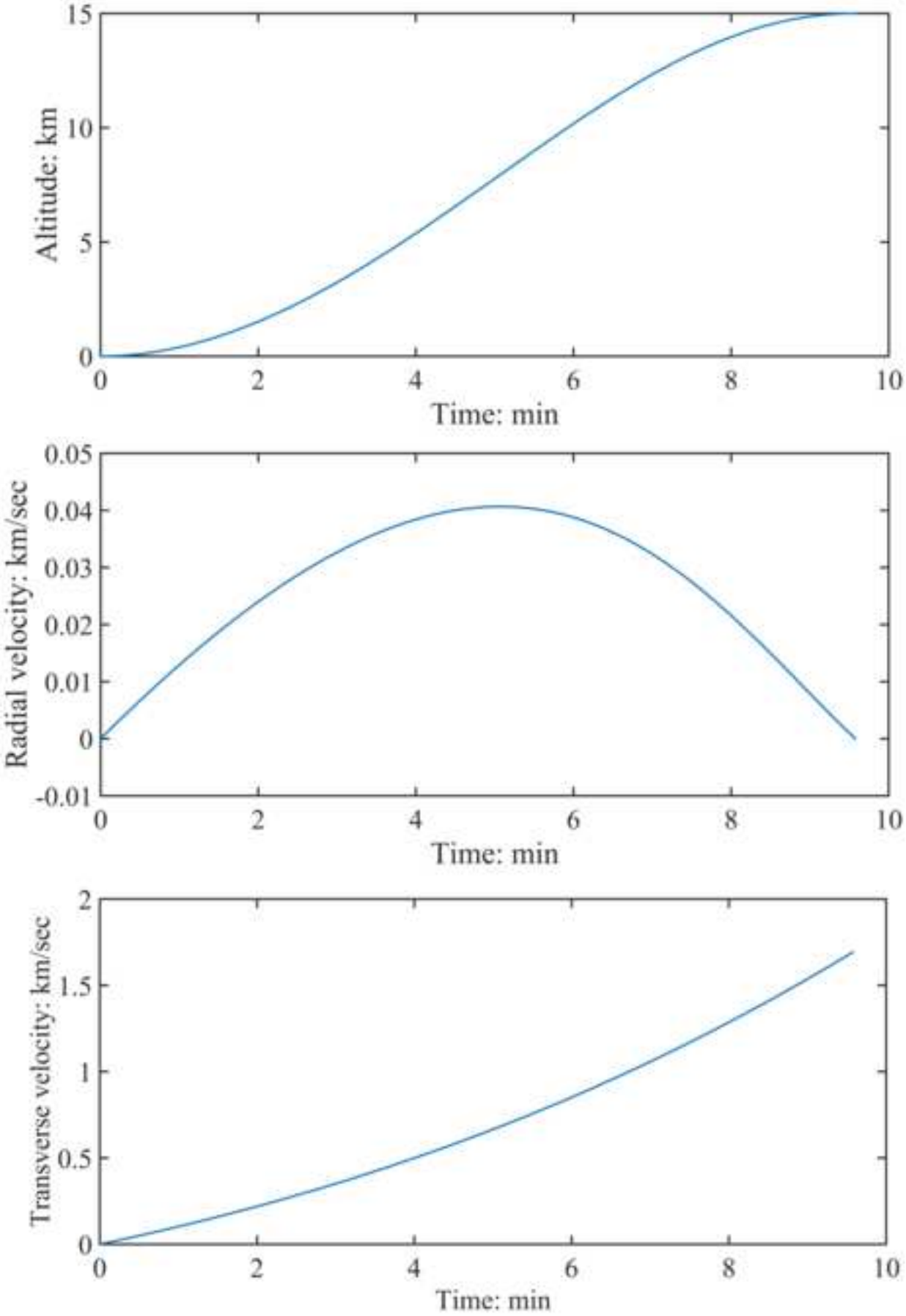

Figure 3

Click here to download Figure figure03.tif

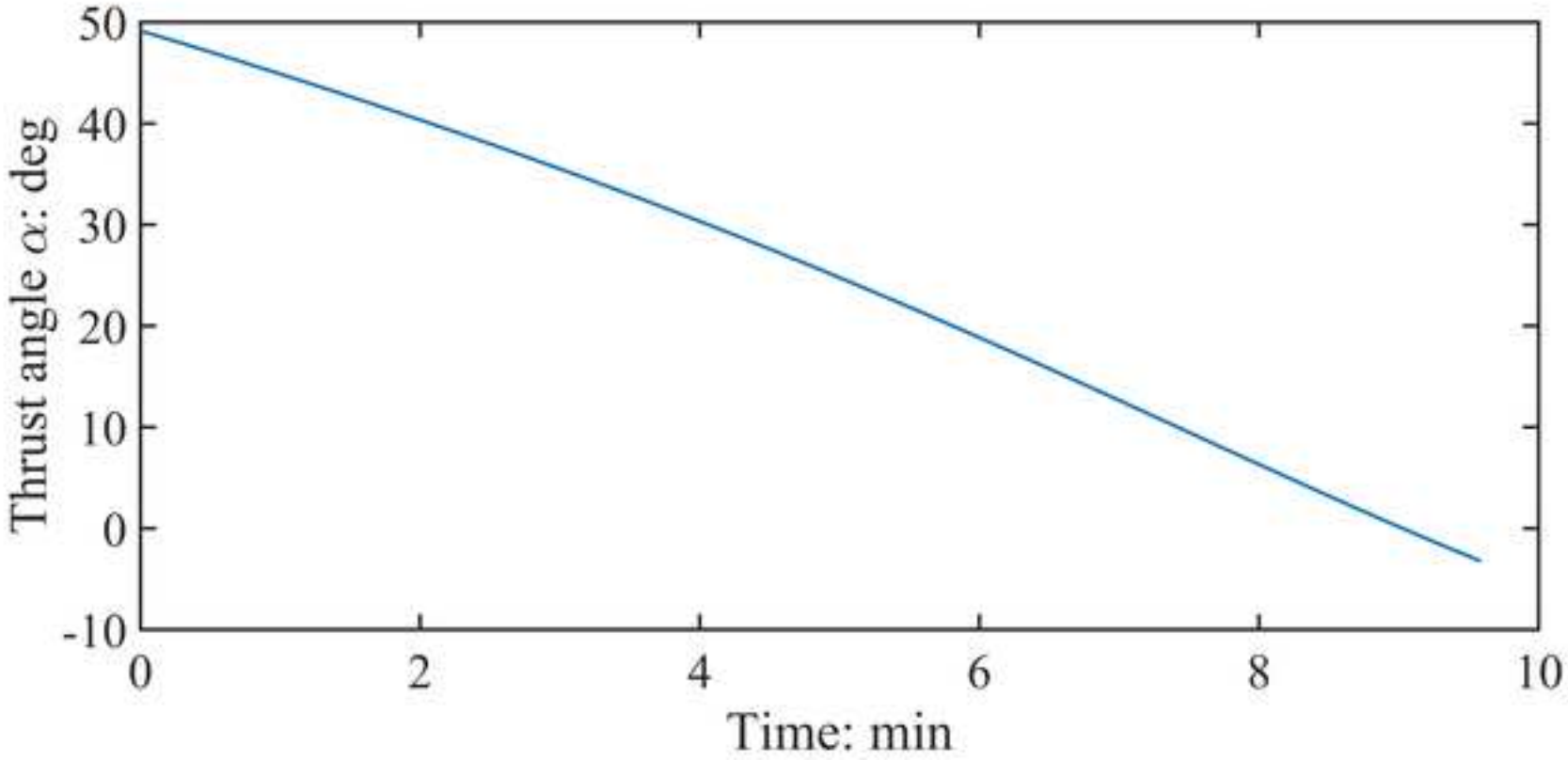

Figure 4

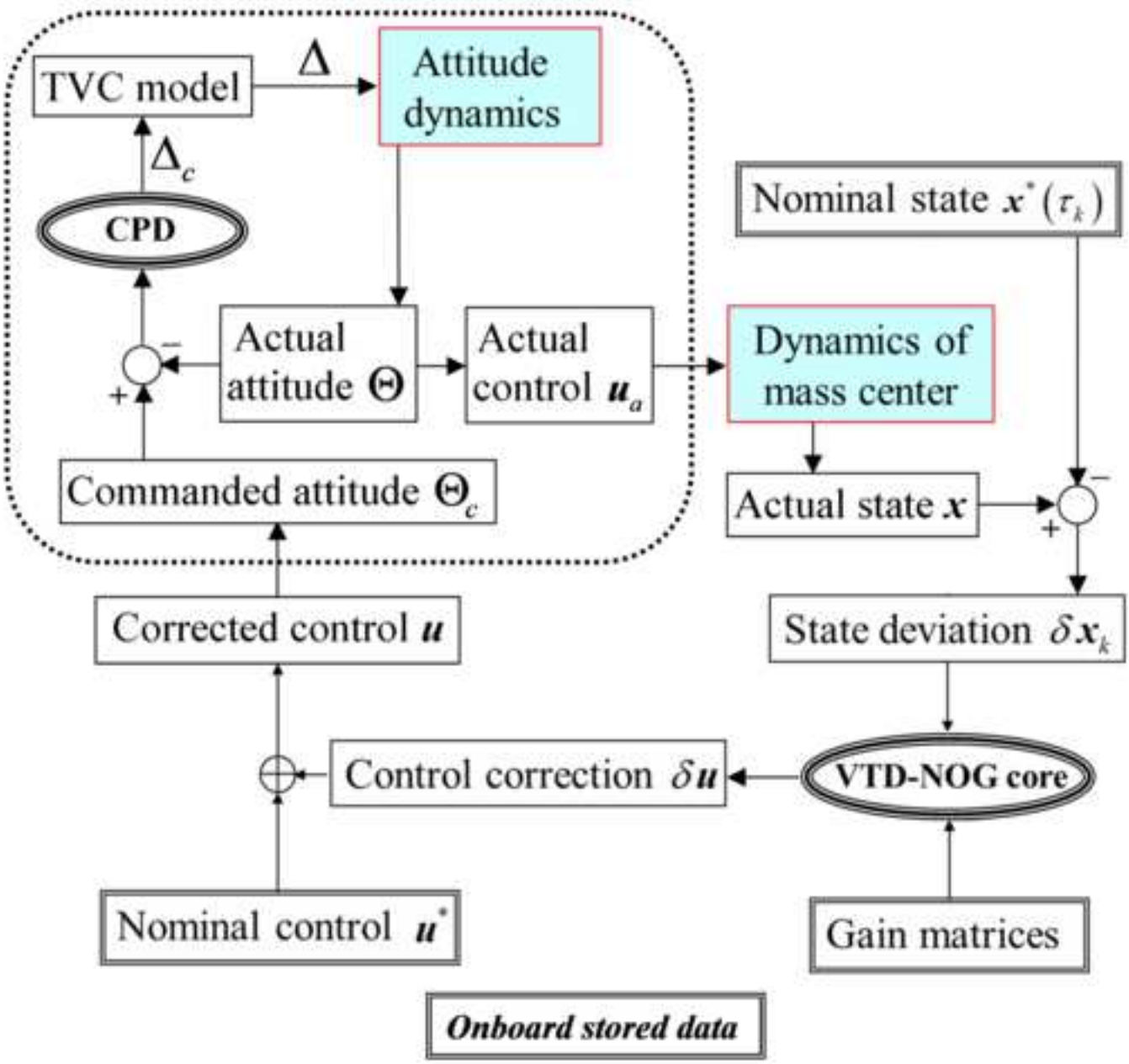

Figure 5

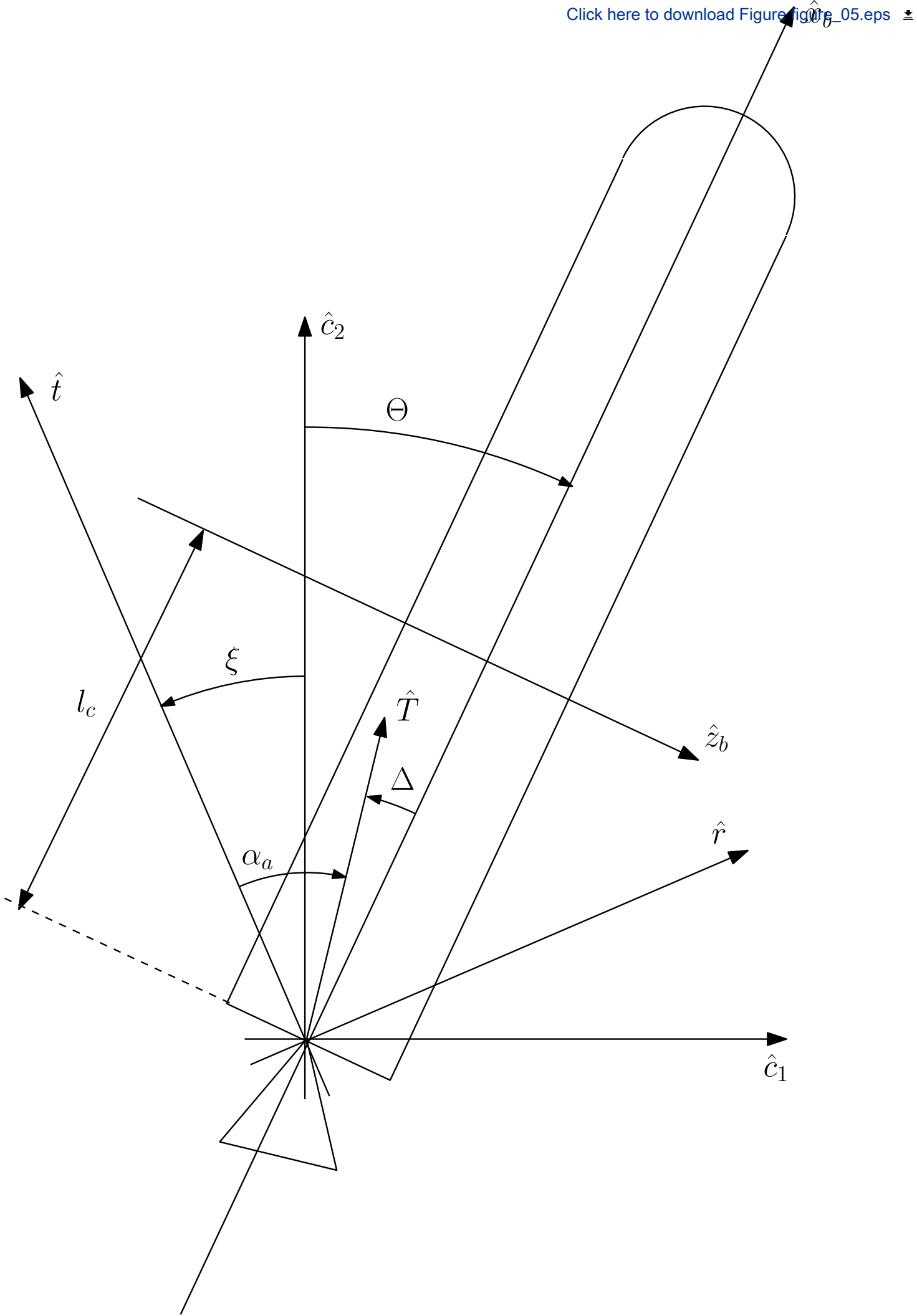

Figure 6

Click here to download Figure figure_06.tif

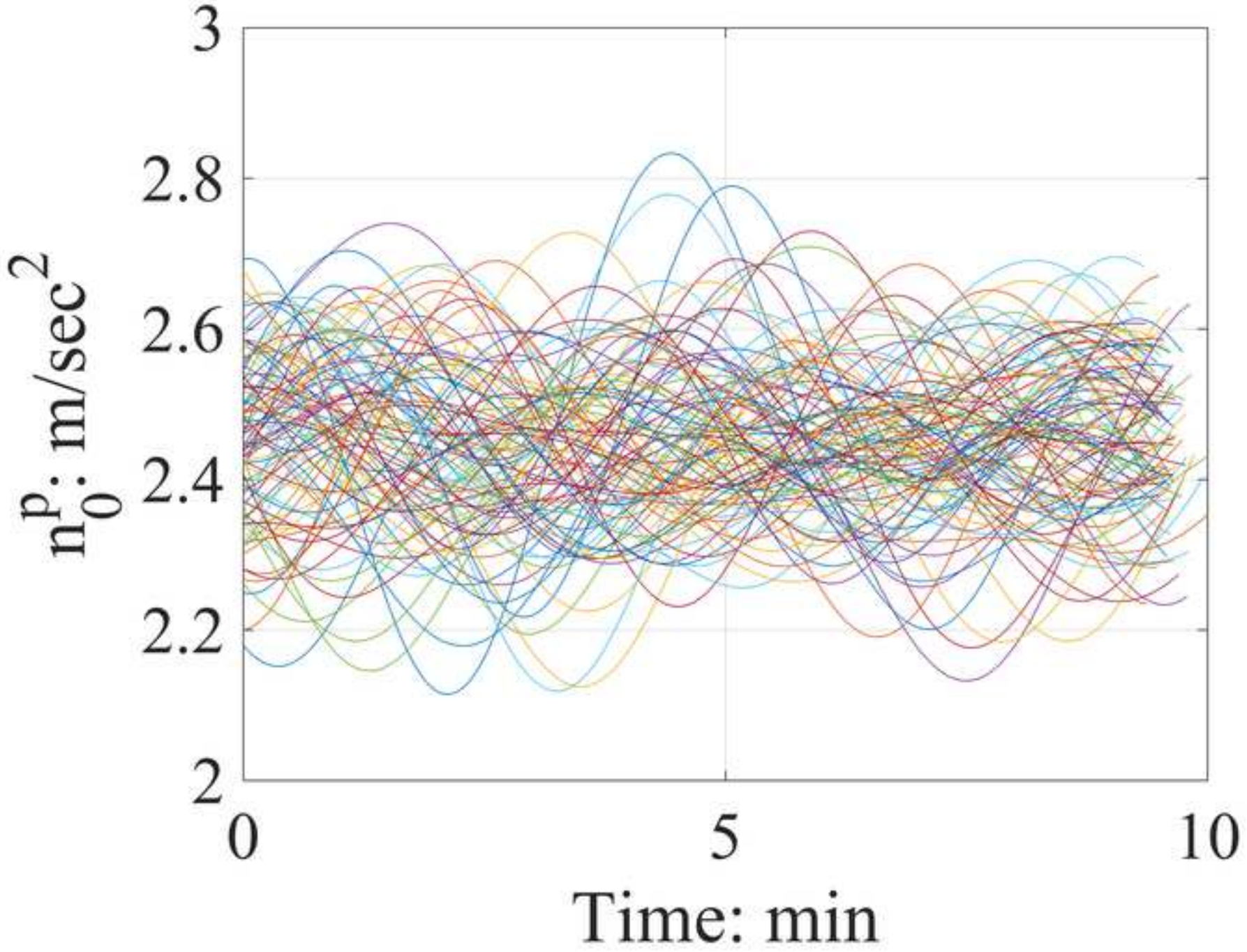

Figure 7

Click here to download Figure figure_07.tif

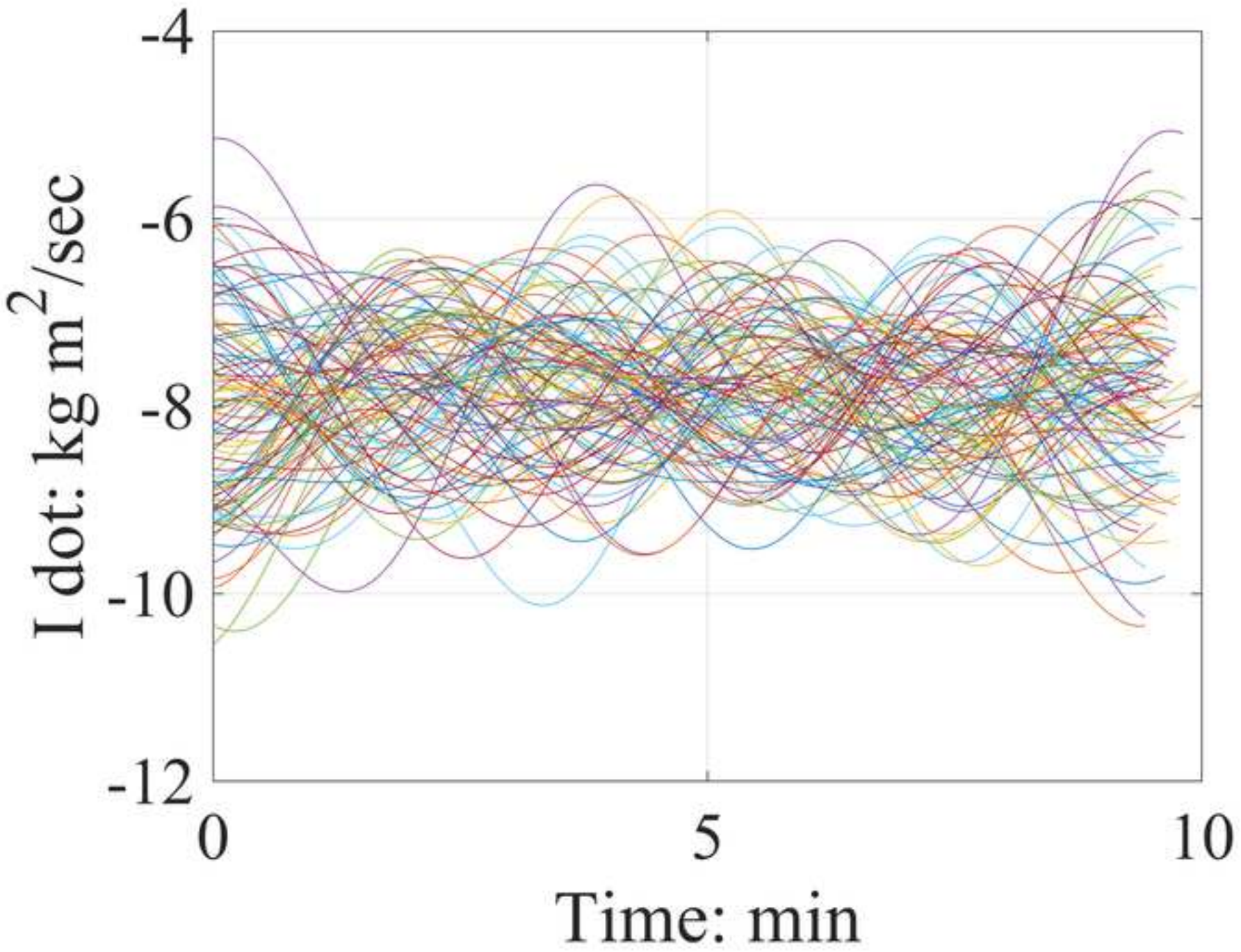

Figure 8

Click here to download Figure figure_08.tif

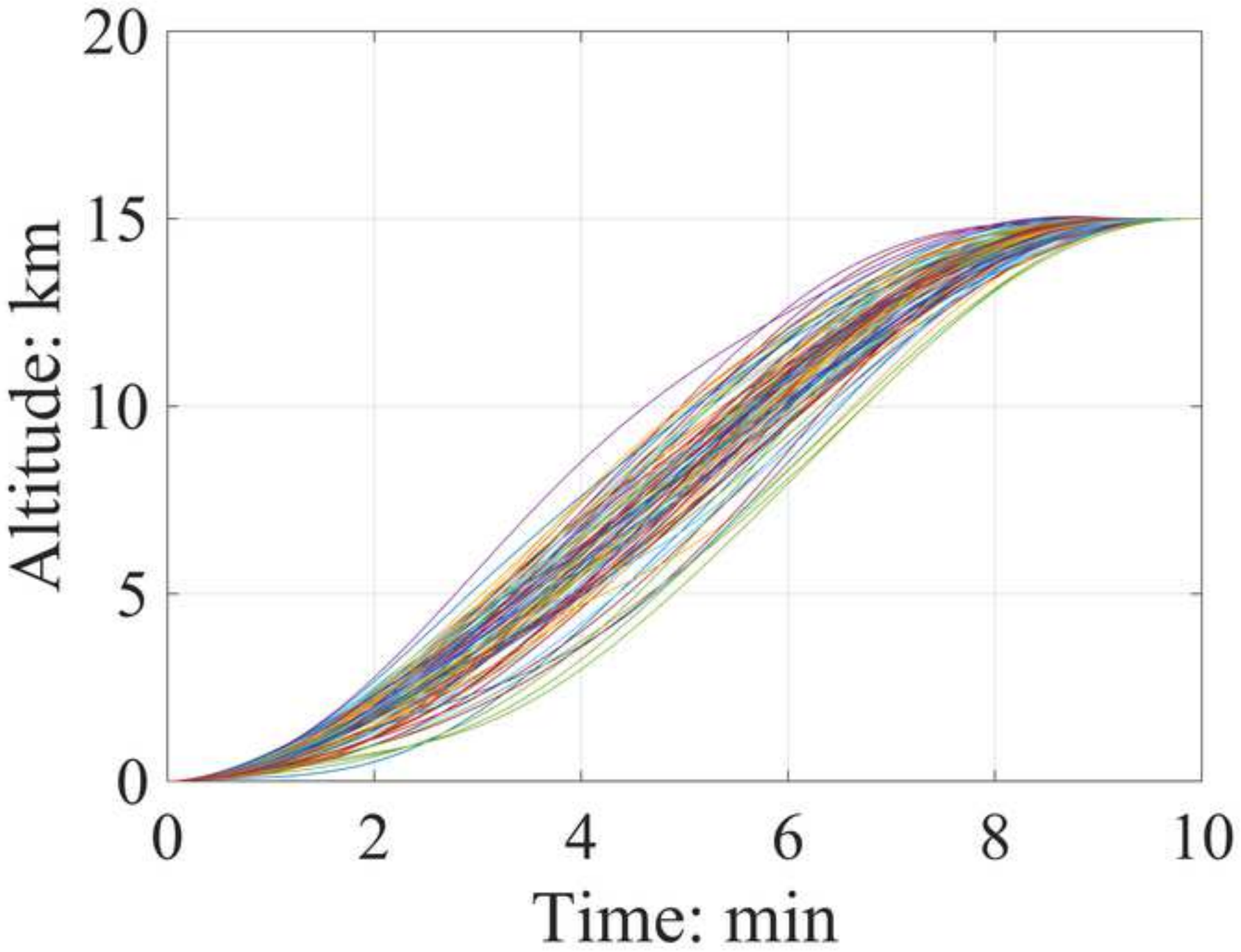

Figure 9

Click here to download Figure figure_09.tif

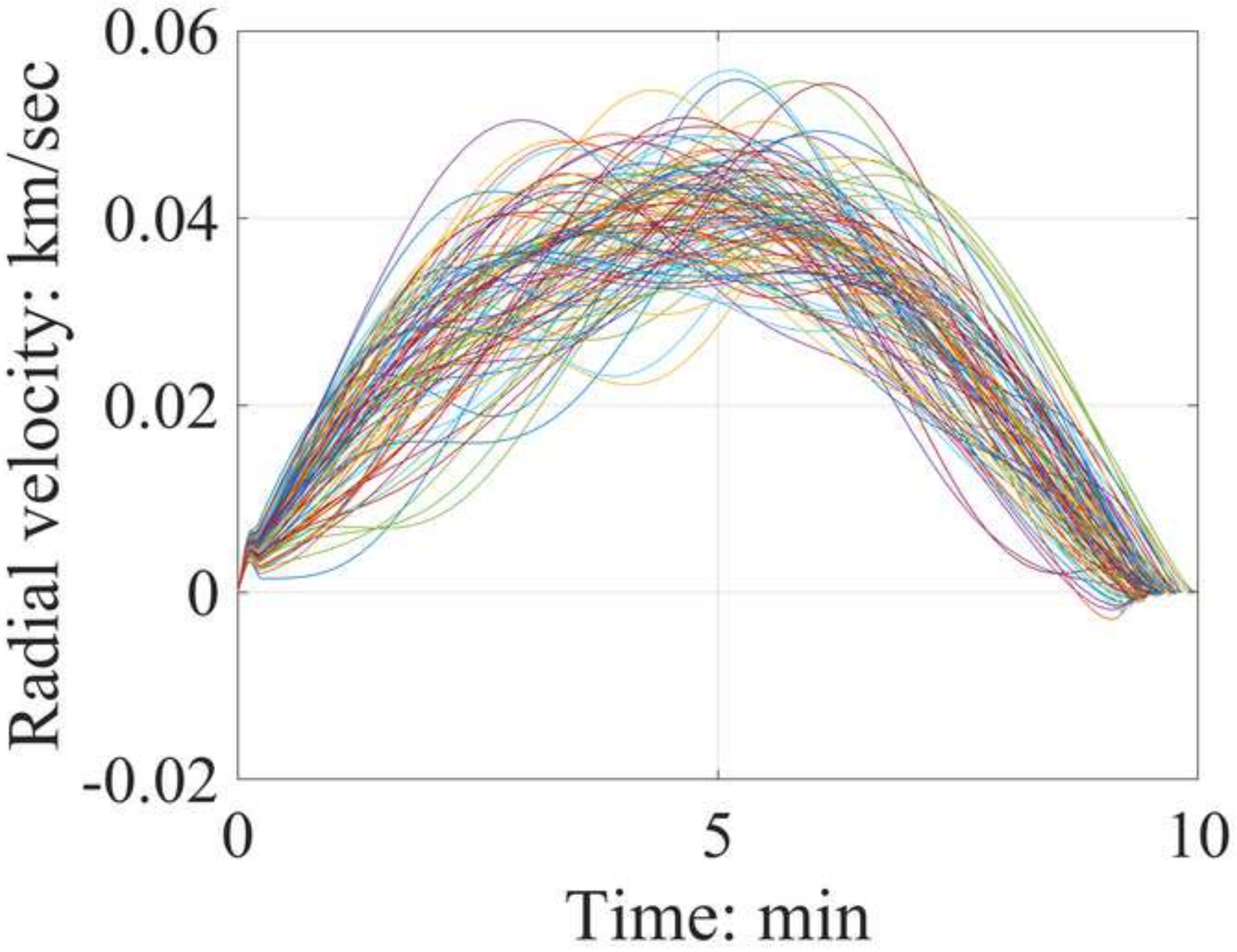

Figure 10

Click here to download Figure figure_10.tif

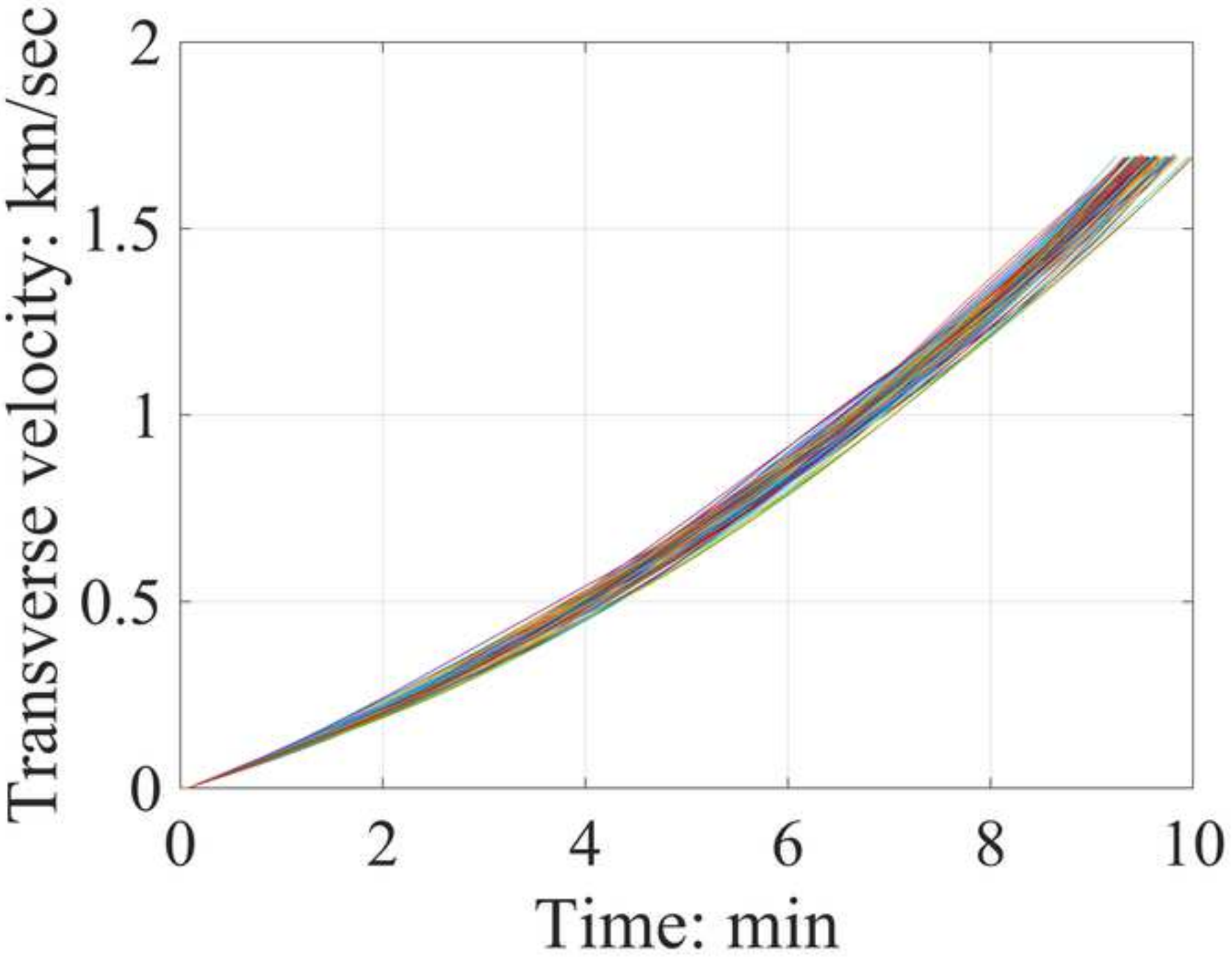

Figure 11

Click here to download Figure figure_11.tif

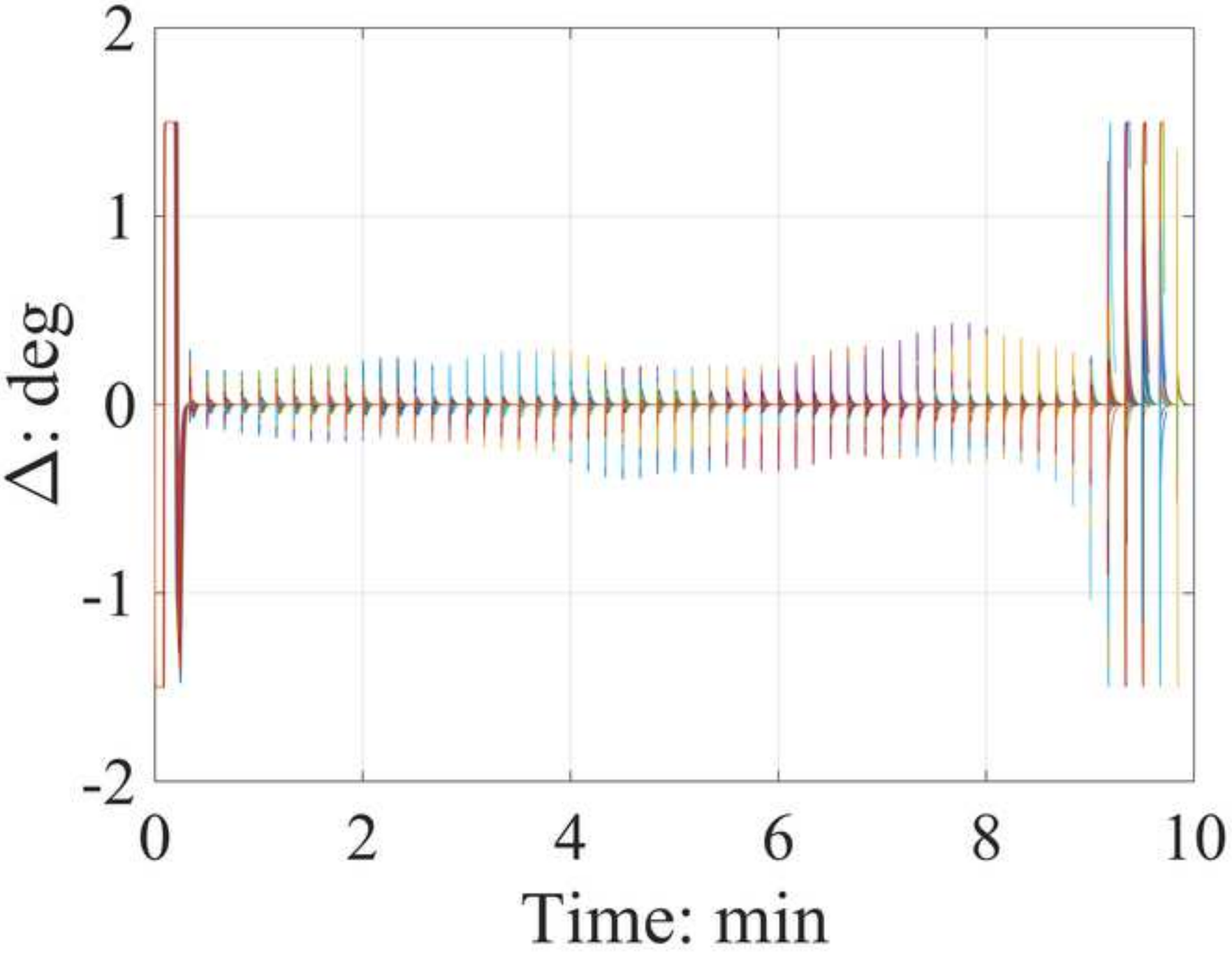

Figure 12

Click here to download Figure figure_12.tif

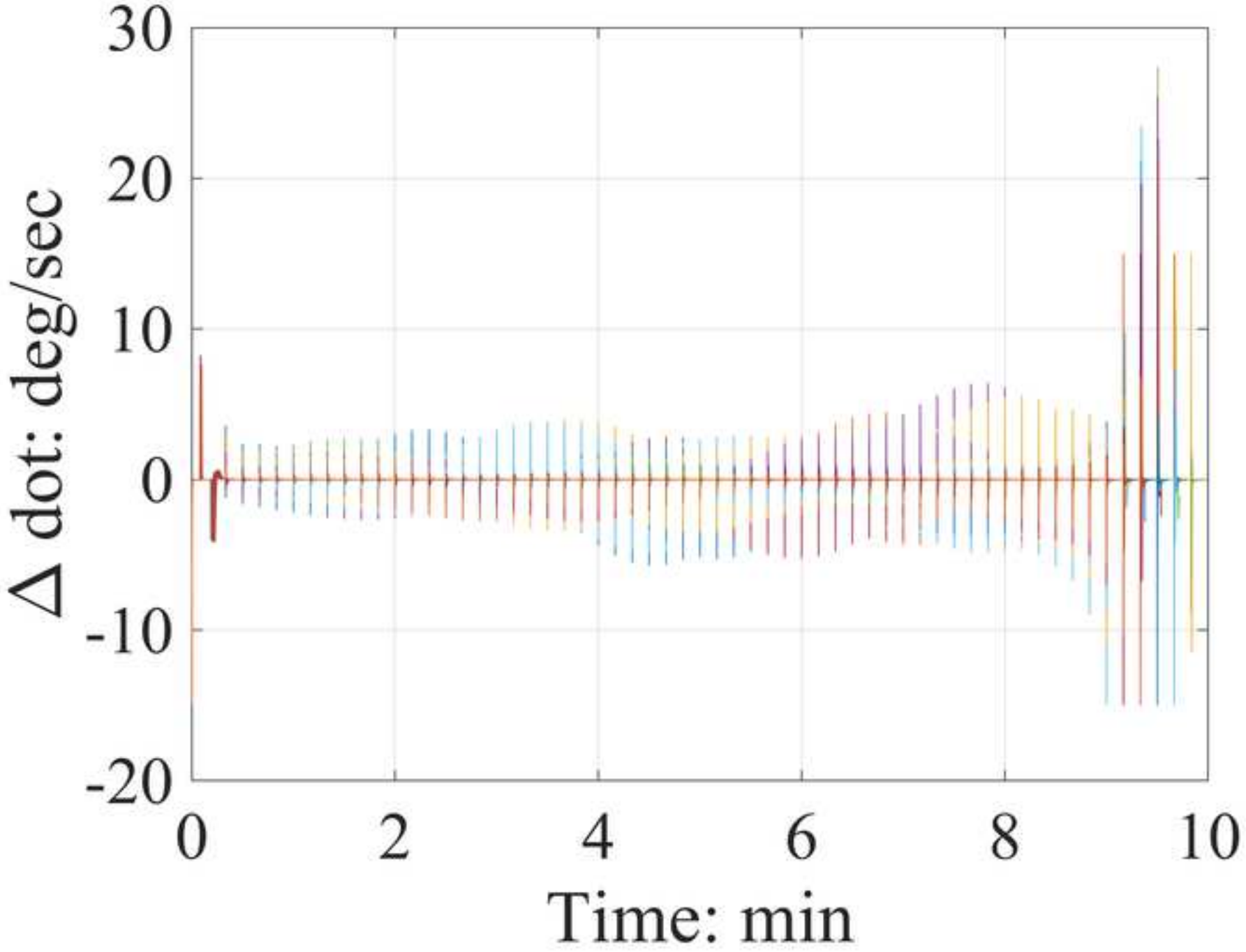

Figure 13

Click here to download Figure figure_13.tif

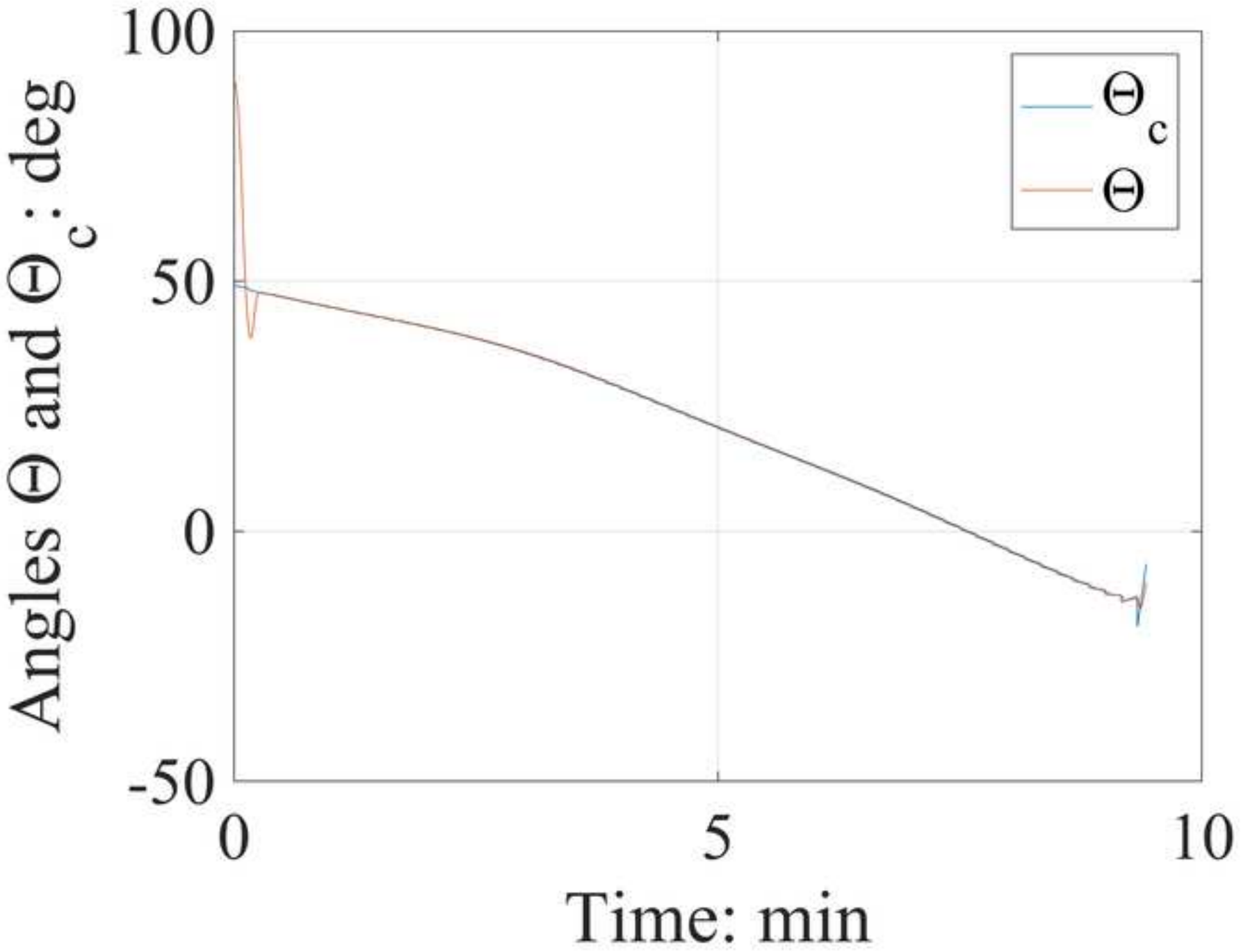

Caption List

1. Reference frame for lunar ascent
2. Optimal lunar ascent trajectory: state time history
3. Optimal lunar ascent trajectory: control time history
4. Block diagram of the VTD-NOG & CPD architecture
5. Geometry of the spacecraft attitude and related angles
6. Perturbed time histories of n_0 employed in the MC3 campaign
7. Time derivative of the inertia moment I in the MC3 campaign
8. Altitude time histories obtained in the MC3 campaign
9. Radial velocity time histories obtained in the MC3 campaign
10. Transverse velocity time histories obtained in the MC3 campaign
11. Time histories of the engine deflection angle obtained in the MC3 campaign
12. Time histories of the engine deflection rate obtained in the MC3 campaign
13. Time histories of the commanded and actual pitch angle obtained in a single MC3 simulation